EXTRACTION AND DENOISING OF HUMAN SIGNATURE ON RADIO FREQUENCY SPECTRA VIA CONDITIONAL GENERATIVE ADVERSARIAL NETWORK

by

SHIYU YANG

A thesis submitted in partial fulfillment of the
requirements for the degree of

MASTER OF SCIENCE IN MECHATRONIC SYSTEMS ENGINEERING

2022

Oakland University
Rochester, Michigan

Thesis Advisory Committee:

Jia Li, Ph.D., Chair
Manohar Das, Ph.D.
Jun Chen, Ph.D.

ACKNOWLEDGMENTS

This research is supported by Air Force Office of Scientific Research through Fund FA9550-21-1-0224.

Shiyu Yang

ABSTRACT

EXTRACTION AND DENOISING OF HUMAN SIGNATURE ON RADIO FREQUENCY SPECTRA VIA CONDITIONAL GENERATIVE ADVERSARIAL NETWORK

by

Shiyu Yang

Adviser: Professor Jia Li, Ph.D.

This thesis proposes an innovative machine-learning-based method to extract compact, accurate, and adequate human signature in residential environment. Our research created a shielding environment by using electromagnetic fields blocking material to attenuate strong signals in the background. SHapley Additive exPlanations were utilized to identify the most human impacted frequency band range, which ensured the spectra acquired later contain adequate information. In order to extract the spectrum that contains mainly human signature information, we trained a conditional-generative-adversarial network to model the shielding effect. Furthermore, a Support Vector Machine model was trained to evaluate the performance of the conditional generative adversarial network model. The proposed method can generate the spectrum containing the human signature which was originally buried in the background. The experimental results show that the extracted human signature in the synthesized spectrum can be identified by the support vector machine classifier with F1 score of 1.0 while the physically shielded spectrum obtained a score of 0.967.

TABLE OF CONTENTS

TABLE OF CONTENTS—Continued

LIST OF TABLES

LIST OF FIGURES

LIST OF FIGURES—Continued

LIST OF ABBREVIATIONS

ML	Machine Learning
LiDAR	Light Detection and Ranging
PRF	Passive Radio Frequency
RF	Radio Frequency
EMF	Electromagnetic Field
SDR	Software Defined Radio
XAI	Explainable Artificial Intelligence
GAN	Generative Adversarial Network
CGAN	Conditional Generative Adversarial Network
SVM	Support Vector Machine
SHAP	Shapley Additive Explanations
IQ	In-phase and Quadrature
SNR	Signal to Noise Ratio
ReLU	Rectified Linear Unit

CHAPTER ONE

INTRODUCTION

1.1 Problem Statement

Human signatures have individualized patterns and are automatic identifications by quantifying the biological characteristics exist in the human signature [1]. Pioneering studies have sensed and captured human signatures in many forms to serve the purpose of human detection or identification. In light of the rapid advances in machine learning (ML) techniques, different forms of human signature have been used in various applications, such as human detection, positioning, identification, etc. Many popular active sensing modalities for human signature collection include camera [2], LiDAR [3], radar [4][5], infrared [6], WiFi-based system with cognitive radio [7], and even device-free in WiFi sensing [8], but all with their own constraints and limitations [9]. Instead of using any of the active sensing methods aforementioned, our research focused on passive radio frequency (PRF) sensing method via two cognitive radio devices. Due to the advantages of low cost, energy saving, and harmless to human health, especially the ability of allowing customized sensing frequency, makes the PRF sensing method ideal for sensing human related frequency band. Our goal in this paper is not only to capture the PRF spectrum contains human signature, but also extract and denoise the human signature from the RF spectrum in order to better serve the purpose of human identification.

The proposed research is based on the assumption that human signature does exist in the form of RF spectrum and varies for each individual human subject. Since the

human signature buried in the RF spectrum tends to be weak comparing to other existing RF signals within a normal environment, we created a shielded environment to block the interference from external electromagnetic fields (EMF). The RF spectra acquired within the shielded environment are considered to be the spectra that consist of mainly human signature, and used as our target of generating the synthetic human signature in ML model training.

1.2 Proposed Solution

In this thesis, I propose an innovative method of extracting and denoising human signature from the RF spectrum captured in a residential environment via software defined radio (SDR) devices. Prior to the training datasets acquisition, explainable artificial intelligence (XAI) technique is applied to identify the most human impacted RF frequency band range, to ensure the captured spectra carry human signature information. To extract the human signature, a conditional generative adversarial network (CGAN) is adapted to simulate the shielding effect and then synthesize RF spectrum that contains mainly the human signature. At the end, a support vector machine (SVM) classifier is trained using the physically shielded spectrum data. The synthetic RF spectrum is sent into the trained classifier to evaluate the quality of the synthetic spectrum. As the result shows, the human subject categories of the synthetic spectrum can be identified by the classifier with 100% accuracy, which indicates the generated spectrum does contain effective human signature. Furthermore, the CGAN structure has several alternative designs to achieve the same function in this thesis. The detailed framework structures, comparison of CGAN training results and framework design strategy are included and discussed.

1.3 Passive sensing

In the engineering world, both active sensing and passive sensing are the remote sensing methods being used frequently to sample energy. Depending on the property of the sensing target subject, surrounding environment condition and the experiment intention, which sensing method should be used can be easily determined. Active sensing has been most strictly defined as sensing that uses self-generated energy to sample the environment, which requires and also results in the emission of a self-generated signal that could potentially interfere with the experiment environment [10]. Passive sensing, on the other hand, sense the input from the subject's physical environment by detecting the energy emitted or reflected by the subject itself without the need of any self-generated signal. As one of the biggest advantages, the passive method not requiring the generation of any active signal, it results in the sensing to be less harmful to the subject than the active sensing method. Even sometimes these two sensing methods exist and serve in the same sensing system, such as camera, in this thesis we focus on using the passive sensing method only.

With harmless, contactless and requiring minimal effort from participants being the nature of passive sensing, this method has been widely developed and applied in many research fields, such as biotechnology, medical and health, environmental studies, structural engineering, and subject detection and recognition, especially in the case of participants or subjects that are sensitive to any self-generated signal and radiation. For example, a recent study which focuses on Identifying patient-specific behaviors to understand illness trajectories and predict relapses in bipolar disorder uses a passive sensing wearable device for data acquisition [11]. This study mentioned that the passive

sensing device features a 3-D accelerometer and gyroscope, and heart rate and heart rate variability with an infrared optical pulse measurement to assess activity and sleep. Being no harm to the participants is one of the major considerations when selecting the sensing device. In another research focusing on mental health study, cell phone has been used as the passive sensing device to obtain data for studying on the impact of smartphone screen use on behavioral and emotional functioning development of preteens [12]. In research regarding strain and crack sensing [13], wireless strain sensors are used as passive sensing devices since it does not generate interference to the environment and building area. Furthermore, passive sensing method coupled with WIFI and internet of things (IoT) has been used on human occupancy detection and activity recognition studies even more frequently. In this human sensing research [14], a Bluetooth beacon and tablet are used as a passive sensing system to achieve human detection and sending real time detection status to host computer. With similar idea, research uses WiFi-based passive sensing system for human presence and activity event classification with the implementation on an SDR platform [15].

There are many published studies electing to use passive sensing method to achieve human detection and recognition based on the human signature captured by the passive sensors within the designated area and specific environment, which indicates that passive sensing is an efficient method to acquire human signature information with minimal negative impact to the participants and experiment area.

1.4 Cognitive radio and PRF spectrum applications

Cognitive radio, which often being referred as software defined radio (SDR), is a radio communication and signal receiving system that can efficiently sample the radio

frequency signal. It has a long history of being used as sensing device for subject signature sampling. Being wireless sensing solution, some of its advantages are not intrusive, lower cost and of fewer privacy concerns [16].

In some of the use cases, the technology named radio frequency identification (RFID) is adopted as the sensing system. In such a system, the SDR serves as a receiver and it is coupled with different forms of tags. For example, in 2016, Lisowski et el. [17] proposed the use of a wireless and battery-free passive sensing platform to detect structural damage. The platform used a standard RFID transponder device that serves as an interface between low-power sensors and RFID reading devices; the sensors were used for damage detection. Their presentation emphasized a novel technique for energy harvesting. This harvesting task was performed by the magnetic field produced by an antenna of the RFID reading device. A few simple structural examples were presented for a demonstration of their proposed system. The authors gave a high mark about the use of this method under remote, difficult-access, or hazardous conditions.

Later on, cognitive radio device works with by designed WiFi or Bluetooth environment became another widely used passive sensing system due to its high sensing accuracy and long sensing distance. In 2018, Li et al. [18] cited the challenges of using existing radio frequency identification tags, wearables, and passive infrared approaches require the user to carry dedicated electronic devices to obtain high detection accuracy and to avoid false alarms. The authors proposed a novel system for non-invasive human sensing by analyzing the Doppler information contained in the human reflections of WiFi signal. The method proposed was believed to be ideal for human sensing because scenario-specific calibrations was deemed not necessary with this system. They used a

software defined radio system to evaluate their method on multiple events. The results indicate that their proposed system worked well for indoor context awareness, “with 95.3% overall accuracy for event classification and 93.3% accuracy for human presence detection”, outperforming the traditional received signal strength approach. Mohtadifar et al. [19] designed a hybrid radio frequency - and acoustic-based activity recognition system to demonstrate the advantage of combining two non-invasive sensors in Human Activity Recognition (HAR) systems and smart assisted living. The hybrid approach as an innovative use in human activity recognitions, according to the authors, employed RF and acoustic signals to recognize falling, walking, sitting on a chair, and standing up from a chair. Experimenting with a vector network analyzer measuring the 2.4 GHz frequency band and a microphone array, the authors extracted the Mel-spectrogram feature of the audio data and the Doppler shift feature of the RF measurements. The experimental results showed that the hybrid method produced recognition accuracy improvement in all classification tested algorithms. All these researches have proven that SDR is a reliable and accurate method of subject sensing in different conditions.

In this thesis, our approach eliminates the needs of any tags and created wireless signal, which appears to be more independent to the supporting conditions than the methods aforementioned. By doing so, it decreases the chance of trafficking with other existing WiFi or Bluetooth bands, and provides flexibility on experiment location selection and setup.

1.5 Subject signature sensing and denoising

Subject signature can be easily captured by various sensing modalities, thus, it has been frequently used as a main parameter in human occupancy detection, activity

recognition and disease identification in many recent publishes. With this being said, the SNR of subject signature can be sampled very differently depending on the sensor being used and experiment environment. More importantly, the subject signature SNR is a direct factor that impacts the detection and recognition results, the lower SNR might lead to ML model collapse or overfit issues. Thus, improving the subject signature sensing method, experiment setup and denoising techniques became critical and essential for subject signature classification related researches.

First introduced by Buades et al. in [20], the image denoising method named Non Local means algorithm is a traditional method used widely before ML technology become popular. This method is based on the natural redundancy of information in images to removes noise. In recent decades, many researches followed the similar structure as their denoising algorithm [21], [22], [23], which is based on the concept of the restored intensity of the voxel, a weighted average of all voxel intensities in the image, where the voxels are selected by metric similarity of patches [24]. However, with the limitation of reducing the resolution of original image and adding additional partial volume effects, this Non Local means algorithm is replaced by other modern ML techniques such as Principal Component Analysis (PCA) and autoencoder.

PCA, as one of the most commonly used unsupervised ML algorithms, is mainly used for dimensionality reduction of data, thus, it became a powerful tool in image denoising and feature extraction. In research [25], it demonstrates that in combination with an appropriate data–driven extraction of relevant information, PCA can be used for denoising of chemical exchange saturation transfer spectrums. The result also shows that

this method successfully achieves the denoising function without losing the essence of its contained information.

Another popular method among all ML denoising methods is autoencoder denoising. When handling non-linear type data, unlike the PCA only consider linear mappable information to features, the denoising autoencoder tends to learn the higher-level data structure in the non-linear space [26], [27]. Some successful examples of using autoencoder on denoising and feature extraction are [28], [29]. In research [28], they let the hidden layer of autoencoder to capture more robust features by reconstructing the input. This method helps them discover a molecular signature composed of multiple genes that can be used to effectively identify lung cancer, shown by their experiment results. In research conducted by Ram et al. [29], autoencoder can also be used to denoise distorted radar signature. The results of this research shows that their proposed algorithm is particularly effective under low SNR conditions and with large errors in the training data labelling.

In this thesis, a physical shielding environment has been established to improve the SNR during sensing, and a CGAN model is proposed to denoise the spectrum that contains human subject signature by simulating the shielding effect. This denoising method duplicates the physical denoising effect and provides robust performance no matter how the experiment area baseline condition changes. Comparing with other ML learning denoising methods, this method has the advantage of allowing the denoising effect to be adjusted by changing the physical shielding effect. Furthermore, unlike the PCA and autoencoder which require separate training of the ML model when encountering changes increase of subject types, the proposed CGAN method can pre-

train the ML model and take the subject label as input by modifying the condition data. This led to a more reliable, consistent and efficient denoising and feature extraction process.

1.6 Generative Adversarial Networks

The state of art ML framework generative adversarial network (GAN) has been first proposed by Goodfellow et al. in 2014 [30]. It is known of its ability of generating synthetic data such as real-world images and audios, by given the input of either random numbers or real-world acquired data. The idea behind this framework is to design two deep learning network, generator and discriminator, which are trained to against each other. Once it has been brought up, the GAN became a new trend of ML technique and has been applied in many applications. Also, modifications to the original framework are developed quickly. Researchers found that the GAN generation can be driven to certain results with specific patterns by adding the scenario information, which is often referred as the condition of GAN. The CGAN model is then preferred by researchers since it requires less training data and contains more information that is brought in with the condition than the original GAN. Many different types of labelling data can be encoded as condition to provide additional information to the GAN.

Researches published in last decade have studied into supply class label with different network structure [21], [31], [32], text descriptions to generate images [33], object location for positioning tasks [34] and even with image directly for image-to-image translation applications [35]. In research [36], they proposed a CGAN based sharpness-aware generative adversarial network to achieve Low-dose CT image

denoising. The main idea is to use a convolutional layer based CGAN network coupled with an additional sharpness detection network to generate the denoised image and then measure the sharpness of the denoised image, with focus on low-contrast regions. This method shows improvement on accuracy of the generated denoised image, especially on most of the low contrast images. However, requiring more data to train the model and not suitable for other dosage level scenarios are the biggest draw backs of this method. Other researches with similar approach to denoise image type data includes denoising GAN for speckle noise reduction in optical coherence tomography images [37], low dose CT image denoising using GAN with Wasserstein distance and perceptual loss [38], and denoising brain MRI with hybrid denoising GAN with synergistic wave-controlled aliasing in parallel imaging [39]. All these researches proposed their own modification to the CGAN model and achieved better accuracy on the denoised image generation, however, their GAN models all have their own limitations, such as the denoising effect decrease on certain regularization parameters setting scenarios, only perform well on low contrast images and be effective only to identify certain diseases. One common issue for these applications is that high precision, expensive equipment is required for data acquisition process, and the denoising effect is greatly dependent on the imaging machine quality.

In research [40], a GAN is trained for denoising ultrafast two-dimensional infrared Spectra. The experiment uses the IR data captured in the ideal condition as the target, and uses synthetic IR spectra by adding random noise as the input during the GAN training process. The discriminator consists of the combination of “convolution-batch normalization-ReLU” layers with additional dropout layers, and the generator consists of

convolutional2D, dropout and batch normalization layers. This GAN architecture follows the famous pix2pix framework that was published by Radford et al. [41]. Comparing with our CGAN architecture, the generator is lack of enough down-sampling and up-sampling process, which leads to the feature cannot be fully extracted. The discriminator has enough layers to extract the feature, however, being easy to be overfit is the biggest issue of this design.

The proposed CGAN framework in this thesis handles 2-dimensional spectrum data and generate the denoised spectrum based on the physical shielding environment setup, thus, it has the advantages of easy access to the data acquisition, not limited to certain environment to setup the experiment and suitable for all types of human subject. The denoising target dataset are acquired by utilizing the inexpensive EMF shielding materials, comparing with the expensive equipment required for sampling the target images in the aforementioned methods, this approach appears to be easier to execute. The denoising effect can also be tremendously improved with the upgrading of the shielding material.

1.6 Thesis Outline

This thesis consists of five chapters. In Chapter Two, the spectrum measurement setup is explained, as well as the machine learning methods used in this paper which are the Shapley Additive Explanations (SHAP), CGAN and SVM classifier. Chapter Three provides information and photos demonstrating the hardware and experiment setup. Chapter Four demonstrates the experiment results, and the discussion of data frequency band range selection result, CGAN training results and SVM classifier identification

accuracy on the CGAN generated dataset and the physically shielded dataset. Conclusion of this thesis are presented in Chapter Five.

CHAPTER TWO

EXPERIMENT DESIGN AND METHODOLOGY

2.1 Spectrum Measurement

In this thesis, the data acquisition process solely relies on software defined radio (SDR) devices for spectrum sensing. Allowing user to configure the sensing frequency range, step size, sampling rate, and the number of samples in In-phase and Quadrature (IQ) data are some of its major advantages, making the SDR device a convenient tool for our research. Specifically, the RTL2832U model has been selected to use throughout our experiment.

Human signature in RF spectrum is normally buried in the noisy background RF signals and difficult to extract. In our experiment, we setup a shielded environment by using EMF blocking materials to minimize the strong RF signal contaminations. With establishing the physical shielding effect, the SDR devices were able to capture the human signature in a greater signal to noise ratio (SNR) in terms of average power at each frequency that is impacted by human. The spectrum recorded inside of the shield, named as shielded spectrum, contains the extracted human signature, thus it is used as target for training the CGAN. Our approach is to learn and recreate the physical shielding effect through a neural network so that human signatures can be extracted and their SNR boosted.

The experiment datasets acquisition process consists of three phases. The phase 1&2 are constructing D_{SHAP-} and D_{SHAP-} used in the two rounds of SHAP analysis, and the phase 3 dataset is constructed for training the CGAN model and SVM classifier.

The first phase dataset D_{SHAP-1} as shown in Table 2 is recorded at a wide frequency band of 2.4-1000MHz in order to fully cover the most human impacting frequencies. In order to ensure our selected band range covers the most human impacted frequencies of different age groups, we captured RF spectrum data on six participants with different ages and medical conditions. The detailed participants information is summarized in Table 1. Then the SHAP result from the first phase weighed in and narrowed down the frequency band of the second phase dataset D_{SHAP-} to 200-800MHz as shown in Table 3. Based on the two phases of SHAP result, the phase 3 datasets are obtained on the 500-600MHz frequency band.

Table 1. Summary of the human subject participants basic information for phase 1 dataset collection.

Human Subject #	**Weight (lb.)**	**Height (ft)**	**Age (yrs.)**	**Gender**
1	170	6.0	21	Male
2	178	5.7	23	Male
3	165	5.6	31	Female
4	160	5.9	38	Male
5	130	5.7	58	Male
6	110	5.6	62	Female

Table 2. Dataset structure and SDR parameters for phase 1 dataset.

	Phase 1
Dataset Notation	D_{SHAP-1}
Frequency Band	24-1000MHz
Sampling Step Size	1.2MHz
Sampling Rate	2.4MHz
Background Condition	With Shield Only
Total Sample Quantity	600
Subjects	Human Subject 1 - 6, & Unoccupied
Data Prepared For	SHAP

Table 3. Dataset structure and SDR parameters for phase 2 dataset.

	Phase 2
Dataset Notation	D_{SHAP-2}
Frequency Band	200-800MHz
Sampling Step Size	1.2MHz
Sampling Rate	2.4MHz
Background Condition	With Shield Only
Total Sample Quantity	400
Subjects	Human Subject 1 & 2, & Unoccupied
Data Prepared For	SHAP

Unlike the phase 1&2 datasets, the phase 3 consists of two datasets, which are the shielded spectrum dataset D_W taken in the EMF shielded area, and the without shield dataset D_{WO} taken at the same location right after the with shield data is captured but while the shield is removed. The detailed phase 3 dataset structure and parameter settings are summarized in Table 4.

For all three phases data acquisition process, there are human subject 1 and human subject 2 participated throughout the experiment. Also, there is unoccupied scenario included in all three datasets. The finalized dataset $D_{SHAP-1}$and D_{SHAP-2} has

total sample quantity of 320 and 400, while the phase 3 datasets D_w & D_{wo} contain 1600 samples in total (800 for each dataset).

Table 4. Dataset structure and SDR parameters for phase 3 dataset.

	Phase 3	
Dataset Notation	D_w	D_{wo}
Frequency Band	500-600MHz	
Sampling Step Size	2.4MHz	
Sampling Rate	2.4MHz	
Background Condition	With Shield	Without Shield
Total Sample Quantity	800	800
Subjects	Human Subject 1 & 2, & Unoccupied	
Data Prepared For	CGAN & SVM	CGAN

2.2 Data Pre-processing

For every RF spectrum collected in our experiments, the sample number per frequency denoted as N, is set to be 4096. Each datapoint on the spectrum is returned as a sampled complex IQ signal ($I + jQ$) represented by two voltage samples, thus, there are $N/2$ pairs of IQ data being collected at each selected center frequency. The average power P in dB at each center frequency f, which is also the amplitude of RF spectrum collected in our experiments, can be calculated as:

$$P(f) = 10\log_{10}\frac{\sum_{i=1}^{N} p_f(i)}{N/2}, \tag{2.1}$$

where the average spectrum power P is a function of f. p_f is the power at each center frequency f and can be calculated as:

$$p_f = \frac{V_f^2}{R}, \tag{2.2}$$

where R is typical input impedance, rated at 50 Ω by the RTL2832U. V_f is the voltage at f and can be calculated as:

$$V_f^2 = \left(\frac{I_f}{255/2} - 1\right)^2 + \left(\frac{Q_f}{255/2} - 1\right)^2, \tag{2.3}$$

where I_f and Q_f is the IQ data collected at f. The raw IQ data captured by the SDR are 8-bit unsigned data, which are normalized to range (−1, 1) in the equation.

Figure 1 shows one of the pre-processed spectrum samples based on the equations provided.

2.3 SHAP on Frequency Band Selection

Our group previous research result indicates that the full frequency band range 24-1760MHz contains adequate information to achieve human occupancy detection [42]. However, due to the data recording and CGAN processing time being too long with the full range spectrum, we aim on developing a process to identify the most human impacting frequency band range to improve the CGAN training process efficiency.

The software package SHAP has been making promising recent contributions on quantifying feature relevance using Shapley values, and it has been proven that the SHAP is suitable in many machine learning scenarios [43]. As a common solution of finding the

most impact factors for the machine learning process, SHAP used in this research is to mainly explain how the impact of the human signature varies at each frequency, and more importantly, to rank out the most human impacted frequencies. There are two phases of dataset prepared for the SHAP as aforementioned, both of them contain the "Human Subject 1", "Human Subject 2", and "Unoccupied" categories, which means the SHAP results are mainly explaining the impact factors when classifying these three categories.

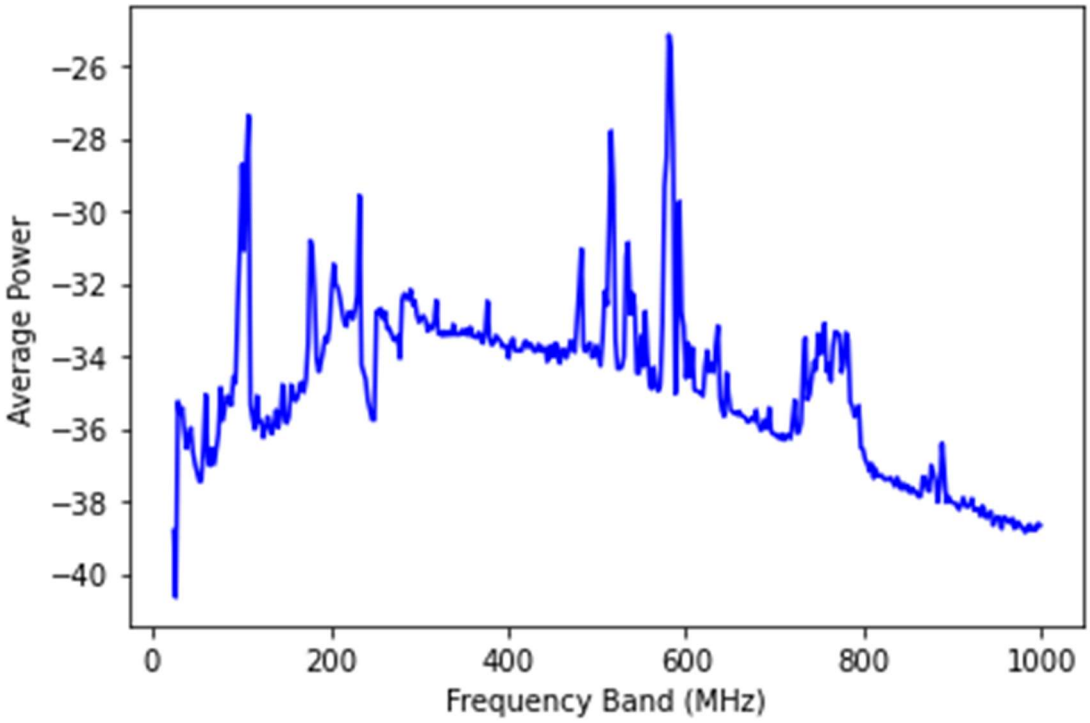

Figure 1. Pre-processed full frequency band spectrum plot.

Prior to the two major rounds of SHAP analysis, full frequency band samples were collected to identify the preliminary frequency band range, which is used to set the frequency band of D_{SHAP-1}. Phase 1 SHAP analysis is then conducted with D_{SHAP-} as the input. A second round of data acquisition and SHAP is performed with narrower frequency band while using the first round SHAP result as the reference, in order to verify the first-round result and further narrow down the frequency band range of phase 3 dataset.

2.4 CGAN Model Structure

A generative adversarial network (GAN) is a class of machine learning frameworks designed by Ian Goodfellow and his colleagues in June 2014 [44], which has the ability of generate new data based on the same data distribution learnt from the training set. On top of the GAN theory and structure, Conditional GAN (CGAN) method adds in the data label and other useful information that can efficiently describe the data to the neural network in order to achieve the same level of generation accuracy but requires fewer data [45]. Due to the data acquisition process is quite time consuming, CGAN is the main method used in this thesis for creating a digital shielding effect to achieve the human signature extraction and denoising.

The CGAN model structure consists of one discriminator and one generator. The goal of using the CGAN is to simulate the shielding effect and then generate the spectrum contains extracted human signature from the environment without any physical shielding setup. In our experiment, we use D_W as the target to train the discriminator, and D_{WO} is fed into the generator as the input data. The condition used in this CGAN model is one-dimensional label of the experiment subject categories and does not contain any feature

information from the subjects. Once the CGAN is fully trained, the generator model is saved and used separately to generate the spectrum with extracted and denoised human signature from the testing data in D_{WO}. The detailed structure of discriminator and generator of the proposed CGAN model are shown in Figure 2.

One thing worth noting is that all the Dense, Convolutional, and Convolutional Transpose layers shown in Figure 2 are followed by a Leaky ReLU layer immediately. At the data processing level, the generator takes the training data in D_{WO} as input, and then send it to a down sampling process. Figure 2 shows the down sampling process consists of four Convolutional 1D with Leaky ReLU layers to achieve the feature extraction and a Reshape layer at the end. The conditioning data is then concatenated with the output from down sampling process and sent into an up-sampling process, which consists of two layers of the Convolutional 1D Transpose and one Leaky ReLU layer. A Reshape layer and one Dense layer are applied at the end to make the output in the same shape as the samples in D_W, which is (43,1).

The discriminator has a simpler setup of achieving the down sampling process since it is basically a binary classifier in terms of the functionality. The discriminator takes half batch of samples from D_W and another half batch of samples from the generator output as input. The input data are concatenated with the conditioning data and then fed into the down sampling process, which consists of three of the Dense and Leaky ReLU layer combinations. The discriminator output is the classification result and will be feedback to the generator.

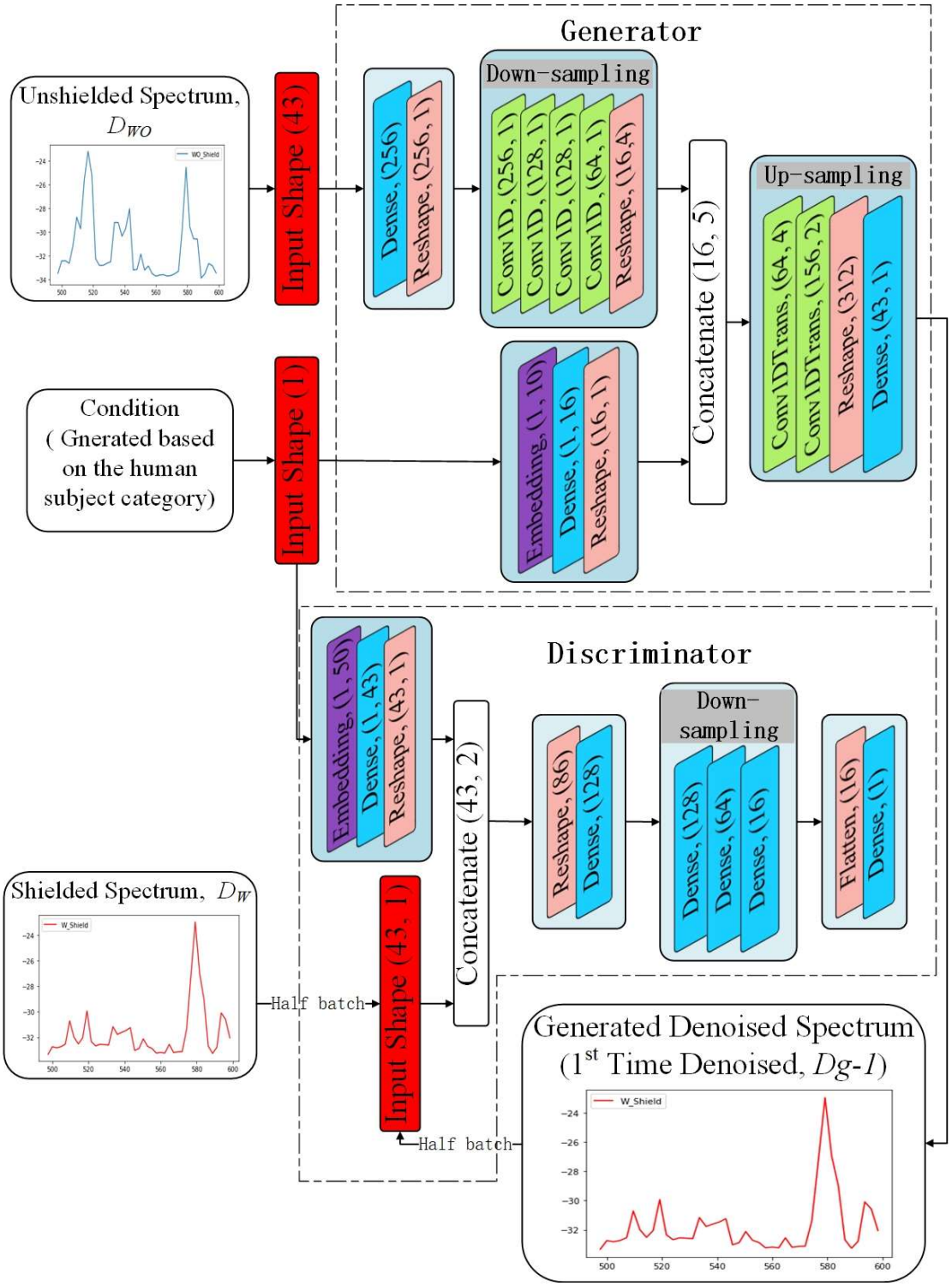

Figure 2. CGAN model structure.

Each sample in the input dataset has 43 datapoints which represent the average power of the 43 frequencies within the frequency band range of 500 to 600MHz, thus, our generator input data shape is (43,1). After the Dense and Reshape layers, the 43 data points are expanded to (256,1). The sample will then go through the down-sampling process and be reshaped to (16,4), and feature extraction happens with the dimension reduction. The condition data with shape of (1) is then concatenated with the sample data and the output data shape is (16,5). The concatenated data will then go through the up-sampling process and the data shape is changed to (312). The purpose of adding this up-sampling process is to handle the data imbalance. Based on the features extracted from the down-sampling process, during the up-sampling process, the neural network will alter the data points and give the useful features a more equal weight. This up-sampling is a critical process in generator training since it ensures all the important features are weighed correctly, which will led to a more accurate output with all the useful features being kept. Later on, our experiment results show that with the up-sampling layers being correctly added, the CGAN obtained better result and has a more efficient training process. The result comparison of the with versus without up-sampling layers is demonstrated in Chapter Four.

In the discriminator, the input data has the same shape as the generator. The condition data is embedded into the same shape as the input data, thus it can be concatenated with the input data. After the concatenation, the data is shaped to (43, 2), and then to be expanded to (128) by a Dense layer. The discriminator only has down-sampling process since it mainly serves as a binary classifier in the CGAN. After going through three Dense layers, the model is enough trained to extract the feature and make

accurate decision on the generator output spectrum. The final output shape comes out of the discriminator is (1), which is the decision been made on classifying the generator output. One thing worth noting is that our discriminator uses Dense layers instead of the Convolutional layer due to our spectrum data type. The main difference between the Convolution layer and the Dense layer is that Convolutional layer tends to force the input share the parameters when learning the relationship of the input and output, it uses fewer parameters by doing so. In contrast to the Convolutional layer, the Dense layer forms every output and corresponding input into a function since it uses linear operation. In our case, as aforementioned the input sample has only 43 data points, meaning there is limited quantity of information and parameters exist in the input data. Also, the dataset sample quantity is relatively small comparing with other CGAN applications since this experiment is not dealing with complicated data type. Considering all these factors, we decided to use Dense layers in the discriminator instead of Convolutional layers since the discriminator does not require heavy loaded learning ability as the generator requires, and the specialty of our dataset as aforementioned. A detailed comparison of the results with two different discriminator setups is presented in Chapter Four.

Optimizing the weights of filters and stride settings is also an important factor of getting good generating result. In the proposed CGAN model, within the down-sampling and up-sampling process, the Convolutional layers strides and number of filters are designed and adjusted based on the CGAN performance. It appears that the CGAN model performs better when the data size increases on the first dimension followed with the data size decreases on the second dimension during the up-sampling process, however, it does not have much effect on the down-sampling process. Some recent GAN related

researches seem prefer to ignore the tunning of this hyper parameter and only use fixed filter size and stride settings. Such as in research [46], it proposes an innovative image denoising method called Residual Encoder-Decoder Wasserstein Generative Adversarial Network. The generator has an encoder-decoder structure composed of 8 layers: 4 convolutional and 4 deconvolutional layers. The paper states that all kernels are set to 3×3×3, and the sequence of the number of filters used is 32, 64, 128, 256, 128, 64, 32, 1. With this one-dimensional changing filter setting, the 3D image data feature is not fully extracted and weighed, since there is only one filter (one dimension of data) being changed to achieve the data shape change flow in the deconvolutional process. When designing and tunning the model, we focused on these hyper parameters and performed various time-consuming tests on different combination, and finally settled with this current setup as shown in Figure 2.

2.5 Evaluation System of the CGAN Model

In machine learning, SVMs are supervised learning models widely used for classification and regression problems, which are ideal and practical for solving linear and non-linear classification problems. Classification based on SVM has been used in many fields like face recognition, diseases diagnostics, text recognition, plant disease identification and intrusion detection system for network security application, and all these related works have proven that SVM is a reliable classification method [13].

For the purpose of evaluating the quality of the generated denoised spectrum, a SVM classifier is trained on the dataset D_W and then used to identify the human subject 1&2 with the generated spectrums. The SVM model has been used here is imported from

the sklearn library with the kernel set to “linear” and probability set to “true”. In Figure 3, the detailed process of utilizing the SVM classifier is further demonstrated.

As Figure 3 shows, the SVM model is trained on D_W, and later on, the trained SVM model is used to classify three sets of data:

a) The testing samples from D_W,

b) The generated denoised spectrum D_{g-1},

c) The generated additionally denoised spectrum D_{g-2},

where D_{g-1} is the first time generated denoised spectrum with D_W being the input, and D_{g-2} is the second time generated denoised human spectrum with D_{g-1} as the input.

In order to generate the D_{g-2} , the generated D_{g-1} is fed back into the trained generator and the output is considered as second time denoised. This process simulates a better shielding effect than the physically shielded environment.

The SVM classification results are expected to be at the same accuracy level on all three sets of data to prove the success of CGAN training. Higher classification accuracy on the synthesized datasets indicates that the trained generator has the ability of extracting real human signature from the measured spectrum in a residential environment without physical shield.

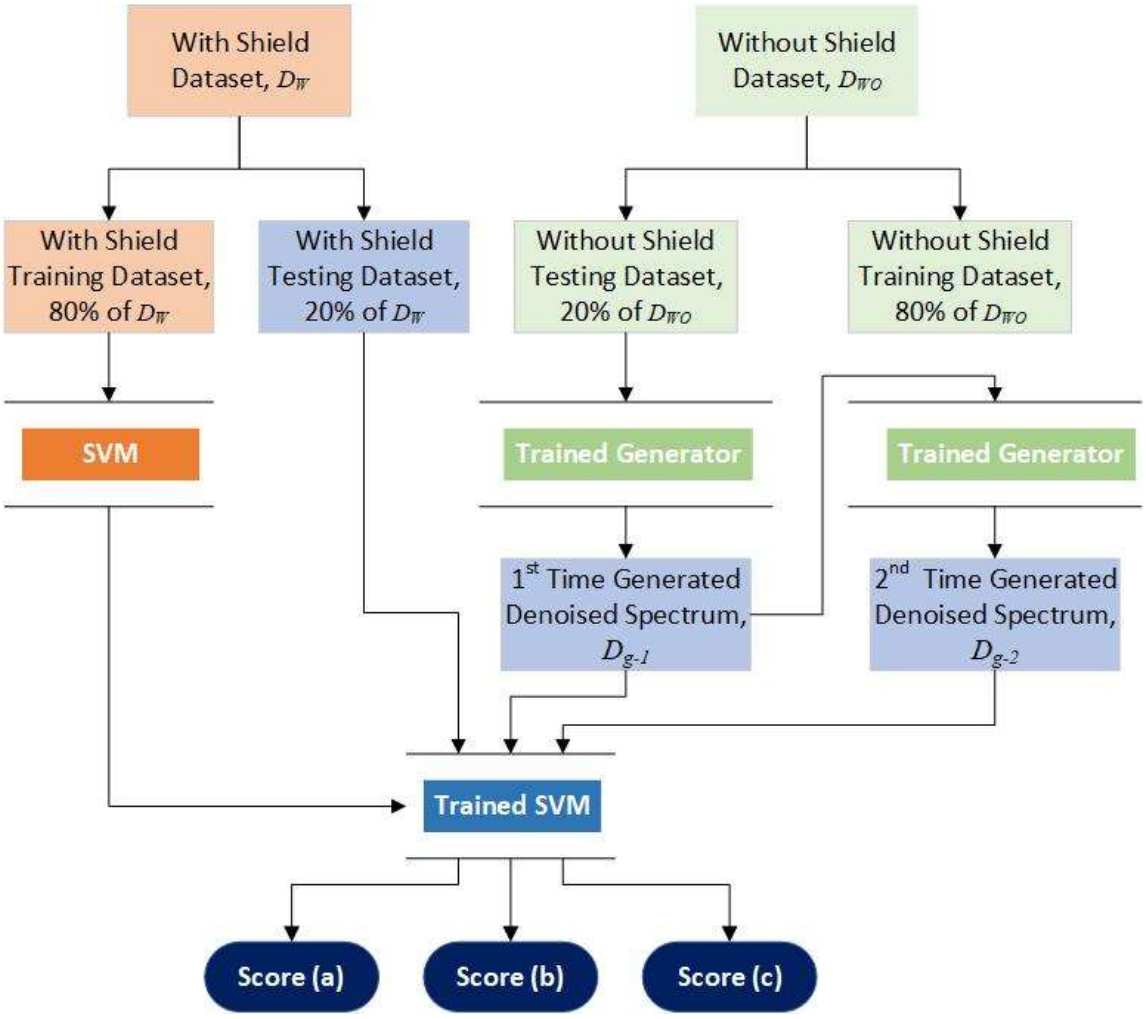

Figure 3. Evaluation system flow chart.

CHAPTER THREE
HARDWARE AND EXPERIMENT SETUP

3.1 Hardware

In the proposed research, the hardware used includes two SDR devices for receiving RF data, one set of RF signal shield, and two pieces of EMF shielding fabric. The detailed product information is further explained in this chapter.

3.1.1 SDR devices

Figure 4 shows the SDR device used in this experiment. This device is named RTL-SDR as it is manufactured by Real Tech, with one of their own RTL2832U chipset to support the software defined feature. The receiving RF band of this device ranges from 500kHz up to 1.7GHz and could be adjusted by software. This SDR device samples the live radio signal on each center frequency defined by the software, and has the ability of recording the signal as data points represented in IQ data format at the corresponding center frequency. In this thesis, the data points belong to one sample are saved in a .pkl file to be used later in data pre-processing.

Figure 4. RTL-SDR device used in the experiment.

3.1.2 RF signal shield

Figure 5 shows the RF signal shield used throughout our experiment. The shield contains two parts: A tent shape net that is hanged on top and covers the entire experiment area, and a mat placed on the floor that is used to ground the shield. The net hanging on top is made by coated silver fiber, with a size of 120×220×220cm, which creates enough space for human subject to comfortably stay in. The grounding mat placed on floor is wired to the ground of the house power outlet, it creates the grounding effect by touch with the metal net. In Figure. 6 it shows the detail of the wired grounding mat.

The main purpose of using this shield is to reduce RF signal interference from the environment at a residential location, in order to create an experiment space to obtain the target data used in training the CGAN model. The human subjects and SDR receivers were set inside of the shield through half of the data acquisition process, while the other half were taken without the shield and used as input data to the CGAN model.

3.1.3 EMF shielding fabric

Since our goal is to create an experimental environment minimizing the interference from RF signals, all the electronic devices are left outside and far away from the designated experiment area. However, data receiving and recording require the usage of host computers, thus these devices are placed outside but close to the shield. The way we dealt with this situation was covering any necessary electronic devices by EMF copper shielding fabric sheets as shown in Figure 7. Each sheet has a size of 100×110cm, its blocking frequency range is 10KHz to 30GHz.

Figure 5. RF signal shield setup.

Figure 6. Detail of the wired grounding mat placed on the floor underneath the experiment area.

Figure 7. EMF shielding fabric.

3.2 Experiment Setup

The experiment was designed to be setup at a residential location to avoid unnecessary EMF interference, which are commonly existed in a laboratory environment due to the heavy usage of electronic devices. Two SDR devices are placed inside of the shield and were maintained with a fixed distance to the shielding boundary and the same pointing direction throughout the entire experiment as shown in Figure 8 and 9. During the data acquisition process, only one human subject was sitting inside of the shield without any electronic devices. The subjects tried to maintain the same sitting posture throughout the duration.

In Figure10, it shows the spectrum measured within the shielded and without the shield. With all the shielding materials utilized, the RF spectrum recorded within the shield and without the shield have significant difference on every center frequency. The difference also varies on different frequencies, which indicates that the shielding effect varies with the RF average power being different.

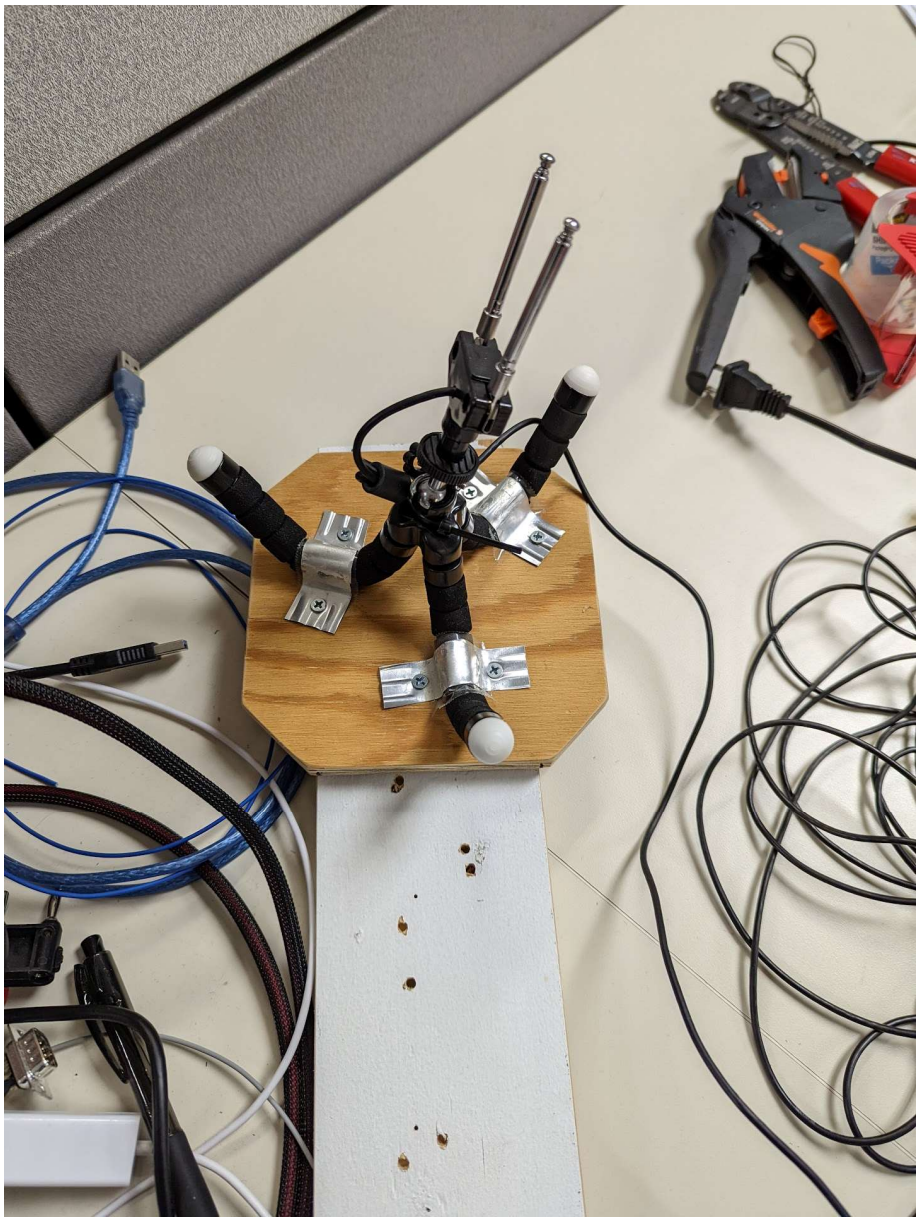

Figure 8. RTL-SDR device mounted on the pedestal with the fixed pointing direction

Figure 9. The setup for human subject data acquisition inside the shield. Two SDR devices were fixed on either side of the human subject and pointing to the human subject.

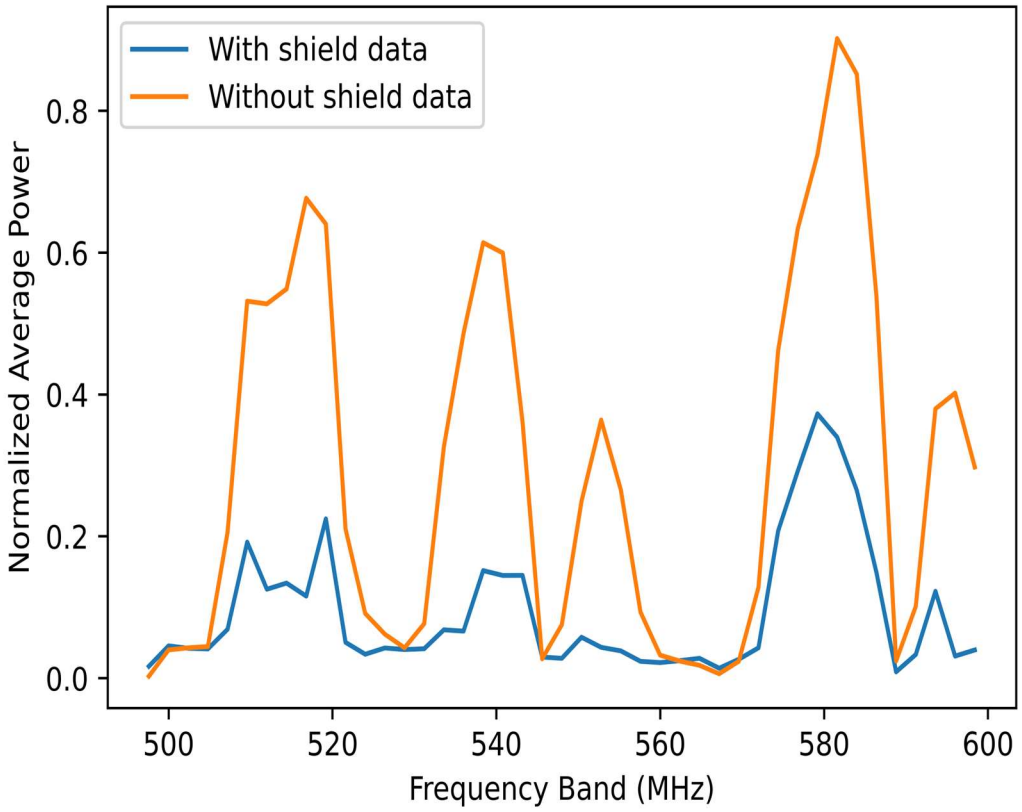

Figure 10. Comparison of the RF spectrum recorded within the shield vs without the shield. This comparison shows the shielding effect of the experiment design.

CHAPTER FOUR
EXPERIMENT AND RESULTS

4.1 Human Impacted Frequency Band

Initially, the spectrum data were taken on full frequency band supported by the SDR, which is 2.4-1760MHz, with 1.2MHz as the step size and sensing frequency set to be 2.4MHz. Due to the data acquisition and processing being inefficient, we adopted SHAP to identify the preliminary frequency band range. Since our research group previous study result shows that the most human impacted frequencies identified by the PCA and RFE-LR have common range of from 500MHz to 700MHz at multiple locations [9], we decided to take small amount of full frequency band data with SHAP to verify this result as our preliminary phase. The SHAP result of this preliminary process shows the top twenty of most human impacting frequencies fall within 100-850MHz, which lead us to set the phase 1 dataset frequency band to 24-1000MHz just to add in some buffer.

The phase 1 SHAP result is shown in Figure 11. The vertical axis shows the ranking of the top twenty most human impacted frequencies, while the horizontal axis indicates the Shapley value of the average power at the corresponding frequency. The dot color represents how the impact value would change as the average power changes. Per the legend at the right side, the dot color in red means the impact value would increase while the sensed human spectrum average power increases at the indicated frequency on the left side, and vice versa. Since the Shapley values are minimal after the top ten frequencies, only the top twelve impacting frequencies are listed and ranked. This result

indicates that all ten most human impacted frequencies fall within the range of 513.2-753.2MHz.

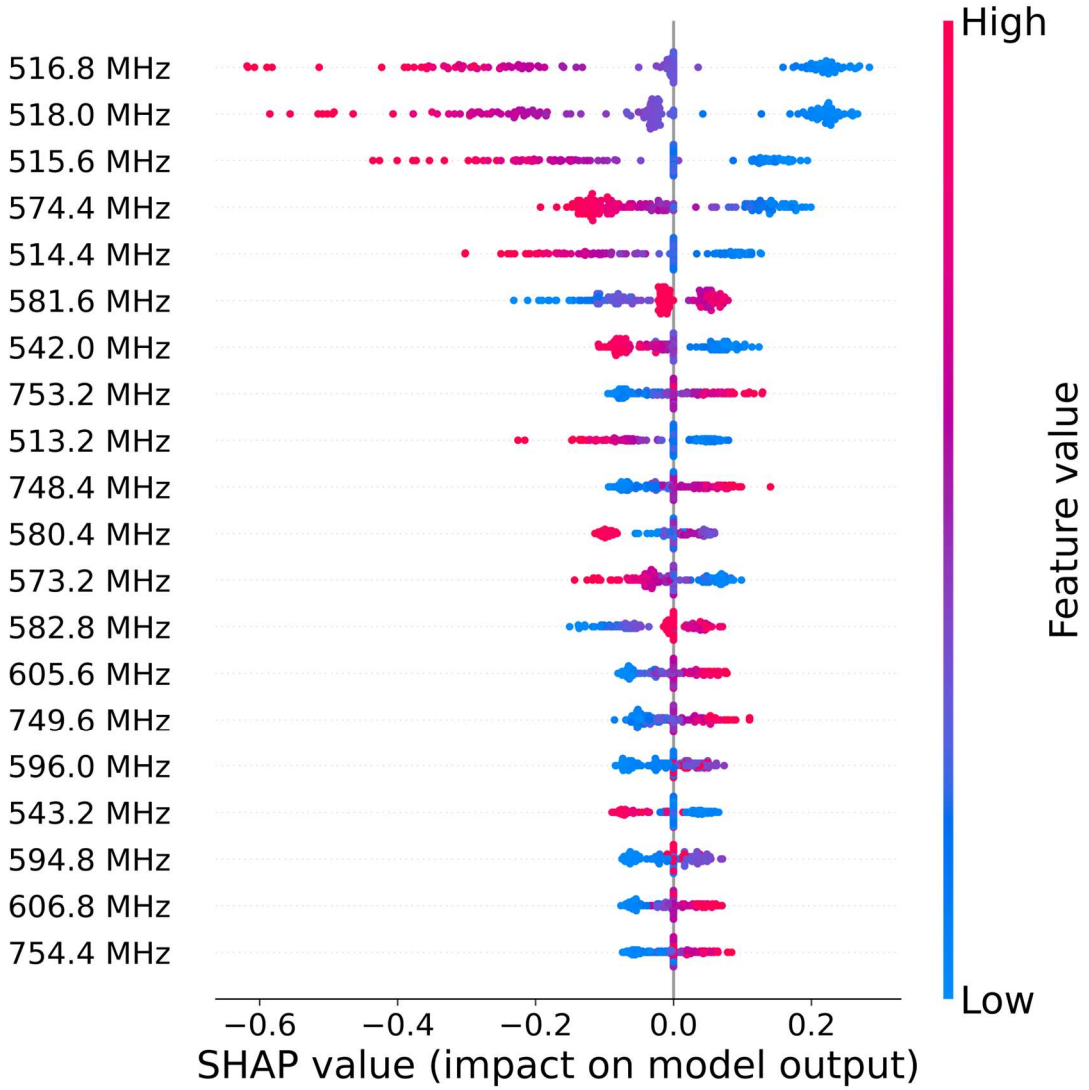

Figure 11. Phase 1 SHAP result.

SHAP was performed again to verify the frequency band selection by using the data acquired in a different time. The target frequency band range has been narrowed

down to 200-800MHz, based on our first round SHAP result. As the second phase result shown in Figure 12, all the greatly human impacted frequencies are within 513.6-597.6MHz. The phase 3 dataset frequency band is then set to be 500-600MHz based on the phase 2 SHAP result. The CGAN training later on proves that this frequency range does contain adequate human signature and provides better efficiency in the training process.

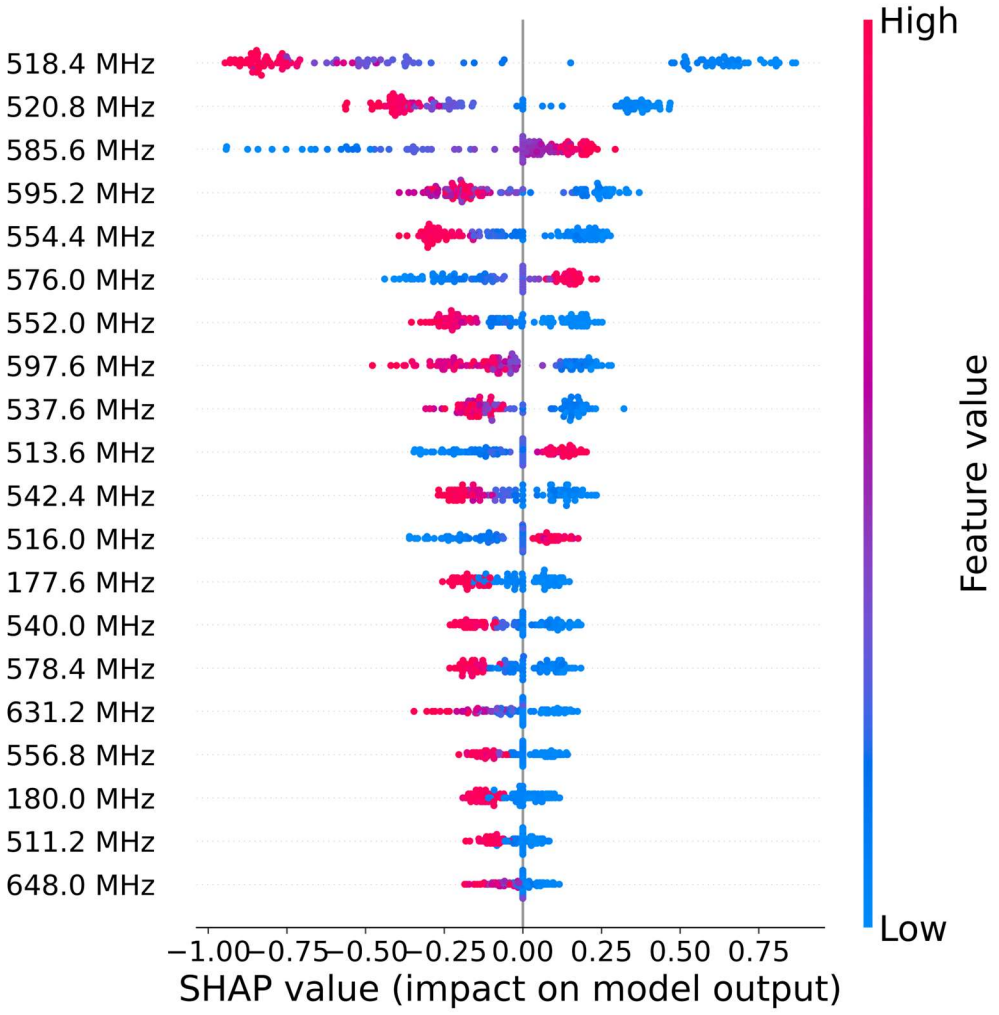

Figure 12. Phase 2 SHAP result.

4.2 Proposed CGAN Training and Synthesized Spectrum

As aforementioned, the unshielded spectrums in D_{WO} contains human signature, but it is also mixed with strong background RF signals. The trained CGAN is able to simulate the shielding effect in order to generate the shielded spectrum from unshielded spectrum. This is a rough human signature extraction process.

Once the datasets are constructed based on the target human impacted spectrum frequency band range, the proposed CGAN model is trained on dataset D_W and D_{WO}. A total of 608 samples in D_W were fed into the discriminator as input and 608 samples in D_{WO} fed into the generator. The CGAN is trained on 220 epochs with a batch number of 20.

Figure 13 shows the loss curve of the training process. The blue and orange lines represent the loss of the discriminator on dataset D_W and D_{g-1}, and the green line represents the loss of the generator, respectively. It can be seen that the discriminator and generator loss were strongly oscillating within 60 epochs of training, which indicates the CGAN model is setup correctly with the generator and discriminator fighting each other at the beginning. The model slowly converges at 60-120 epochs range.

From the CGAN modeling process, our training result shows that any forms of the Keras library built in normalization layer are not benefiting the training process. The proposed CGAN model does not contain any normalization layers, the general data normalization has been performed manually in the data pre-processing phase.

Also, our experiment results indicate that performing the discriminator training first and separately would increase the efficiency of the CGAN training process. This

theory requires adding an additional discriminator training process prior to the whole generator and discriminator coordinated training for every training cycle.

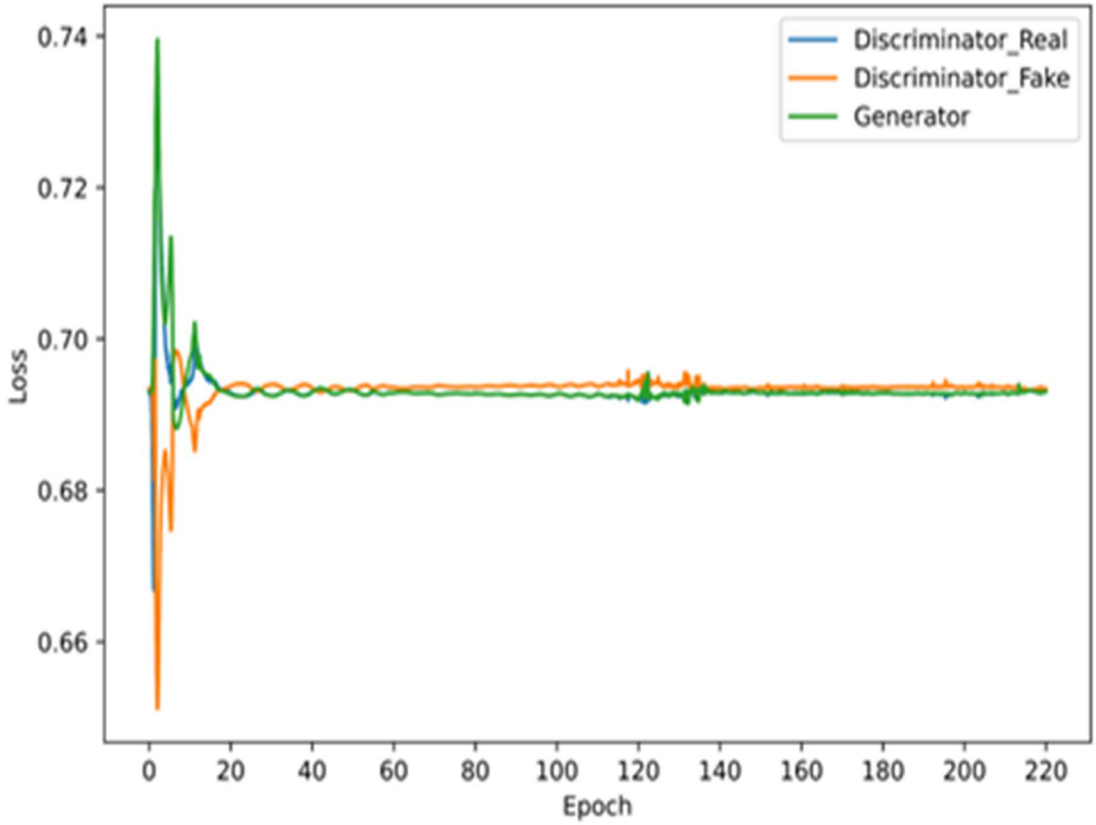

Figure 13. The CGAN training loss curve.

Figure 14 shows the result of the generated denoised spectrum along with the sample from D_W which represents the denoised target spectrum, and the sample from D_{WO}, which is the generator input. These generated first time denoised spectrum construct the dataset D_{g-1}. As it can be easily visualized, the generated spectrum is quite

close to the target shielded spectrum in terms of shape and value, but only with small deviations at the most human impacted frequencies. As discussed later on in Chapter 4.3, the evaluation result implies that the deviations are improvements on the SNR of human signature as D_{g-1} yields better classification result.

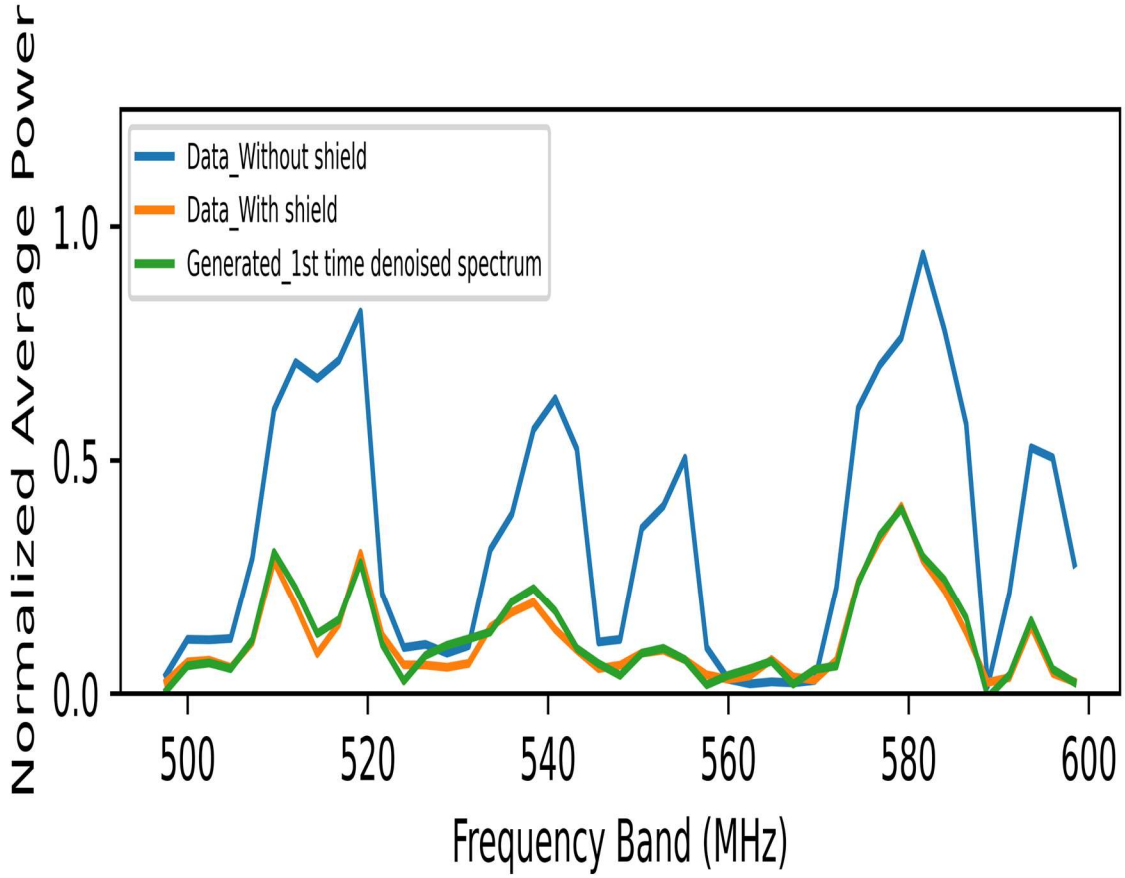

Figure 14. Comparison of sample spectrums from $\boldsymbol{D_W}$, $\boldsymbol{D_{WO}}$ and the synthesized when CGAN is applied the 1st time.

The constructed D_{g-1} is fed back into the generator to generate the second time denoised spectrums and construct the dataset D_{g-2}, and this process simulates a better shielding effect than the physically shielded environment. Figure 15 summarizes the second time CGAN generation results, including spectrum samples from D_{WO}, D_W and D_{g-2}.which are represented by the blue, orange and green lines in the figure. The purpose of computing this graph is to visualize the improvement of the denoising function achieved by the second time generation.

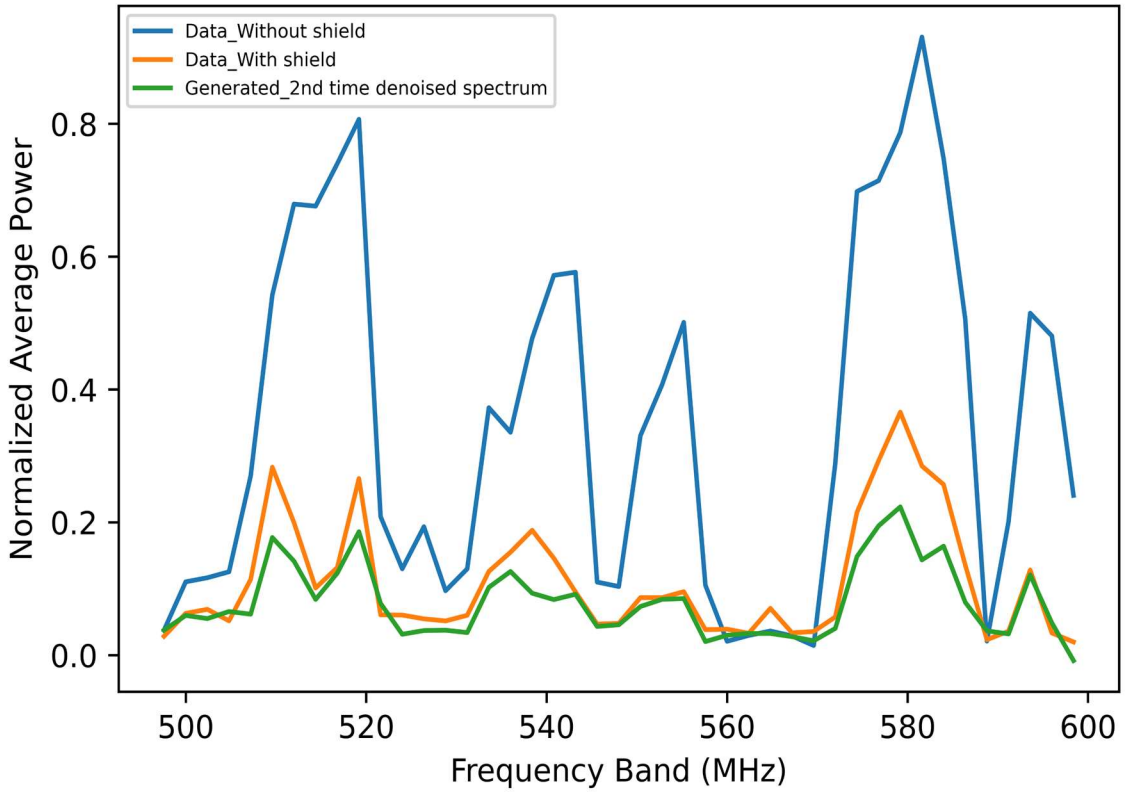

Figure 15. Overview of the generation results. It shows the comparison of sample spectrums from $\boldsymbol{D_{WO}}$, $\boldsymbol{D_W}$ and the synthesized when CGAN is applied the 2nd time.

Based on the result shown in Figure 15, it is obvious that the generated spectrum average power has decreased when CGAN is applied the second time, and the decrease amount varies at different frequencies. our initial goal was to train the generator to detect which portion of the spectrum contains the critical human signature and how much noise should be filtered out from the spectrum input based on the pattern that the generator has learnt from the shield. This result satisfies our initial expectation for the generator. After the CGAN is applied the second time, the SNR of the spectrum is further denoised. Multiple stages of denoising is commonly used in signal processing pipeline. To the best of our knowledge, it is the first time that CGAN has been trained and used to achieve the two times denoising function. One of the biggest advantages of this proposed denoising method is that the further denoising function can be easily achieved by applying the trained generator multiple times with newly generated spectra as input, not only limited to the two times denoising.

Figure 16 summarizes the CGAN generation results from this thesis, it contains the spectrum samples from $D_{WO,}$ $D_{W,}$ $D_{g\text{-}1}$ and $D_{g\text{-}2.}$ This figure provides an overview of the multistage denoising and comparison of the target spectrum with the first time generated denoising spectrum.

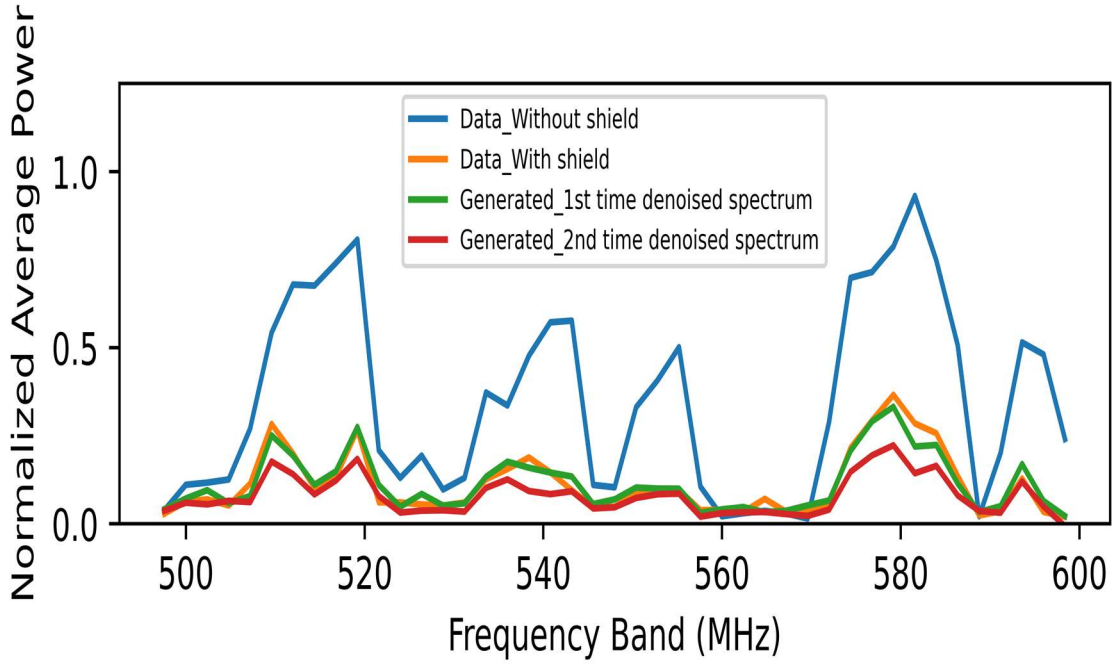

Figure 16. Overview of the generation results. It shows the comparison of sample spectra from $\boldsymbol{D_{WO}}$, $\boldsymbol{D_W}$ and the synthesized when CGAN is applied the1st and 2nd time.

4.3 CGAN Framework Alternatives and Comparisons

In Chapter Two, there are two CGAN framework alternatives have been discussed, which are:

1) Using Convolutional layers in the discriminator down-sampling process instead of Dense layers;
2) Removing the up-sampling process in the generator structure.

The detailed structure of the two alternatives is shown in Figure 17 and Figure 18 respectively.

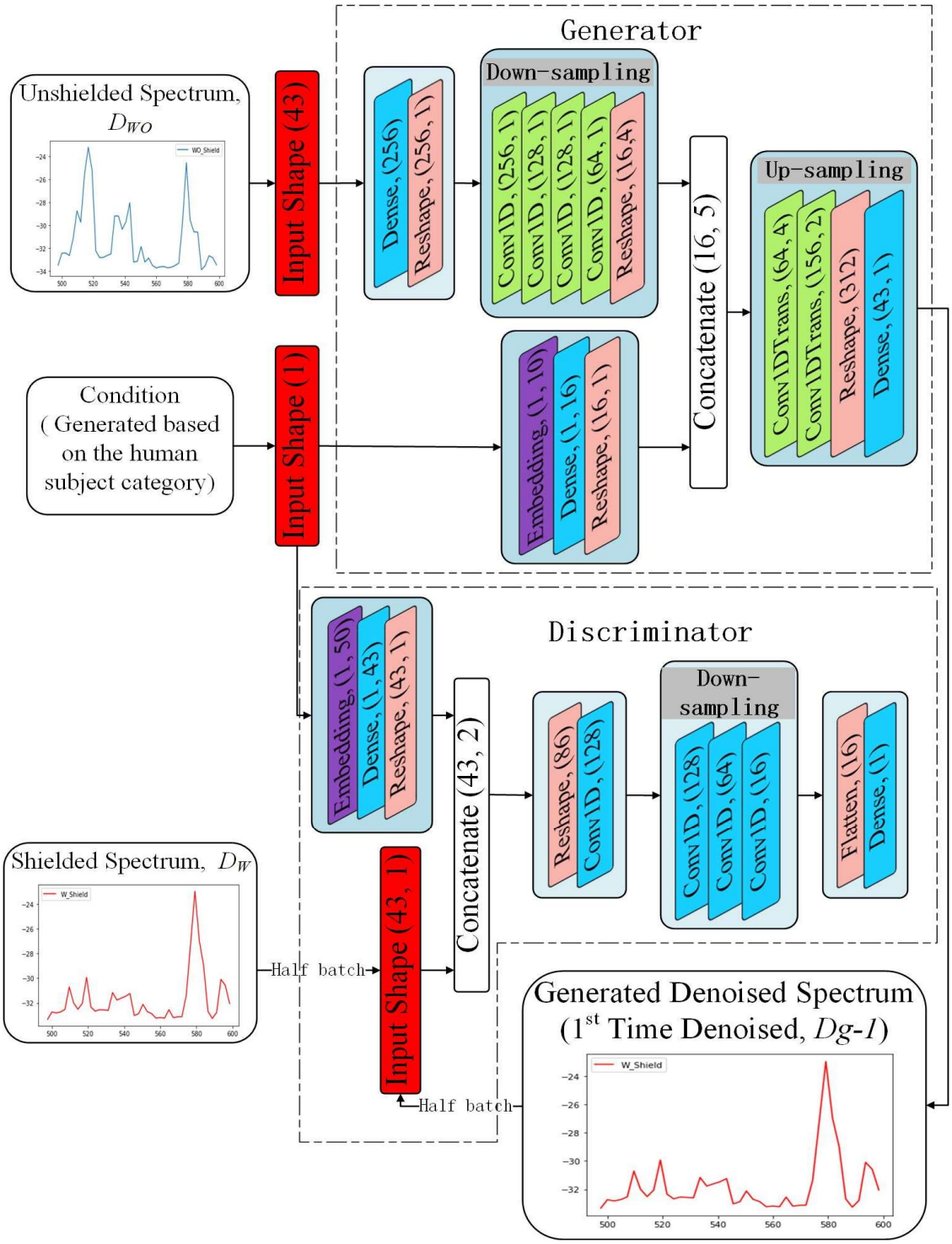

Figure 17. CGAN alternative framework 1: Replacing the Dense layers to Convolutional layers in the discriminator.

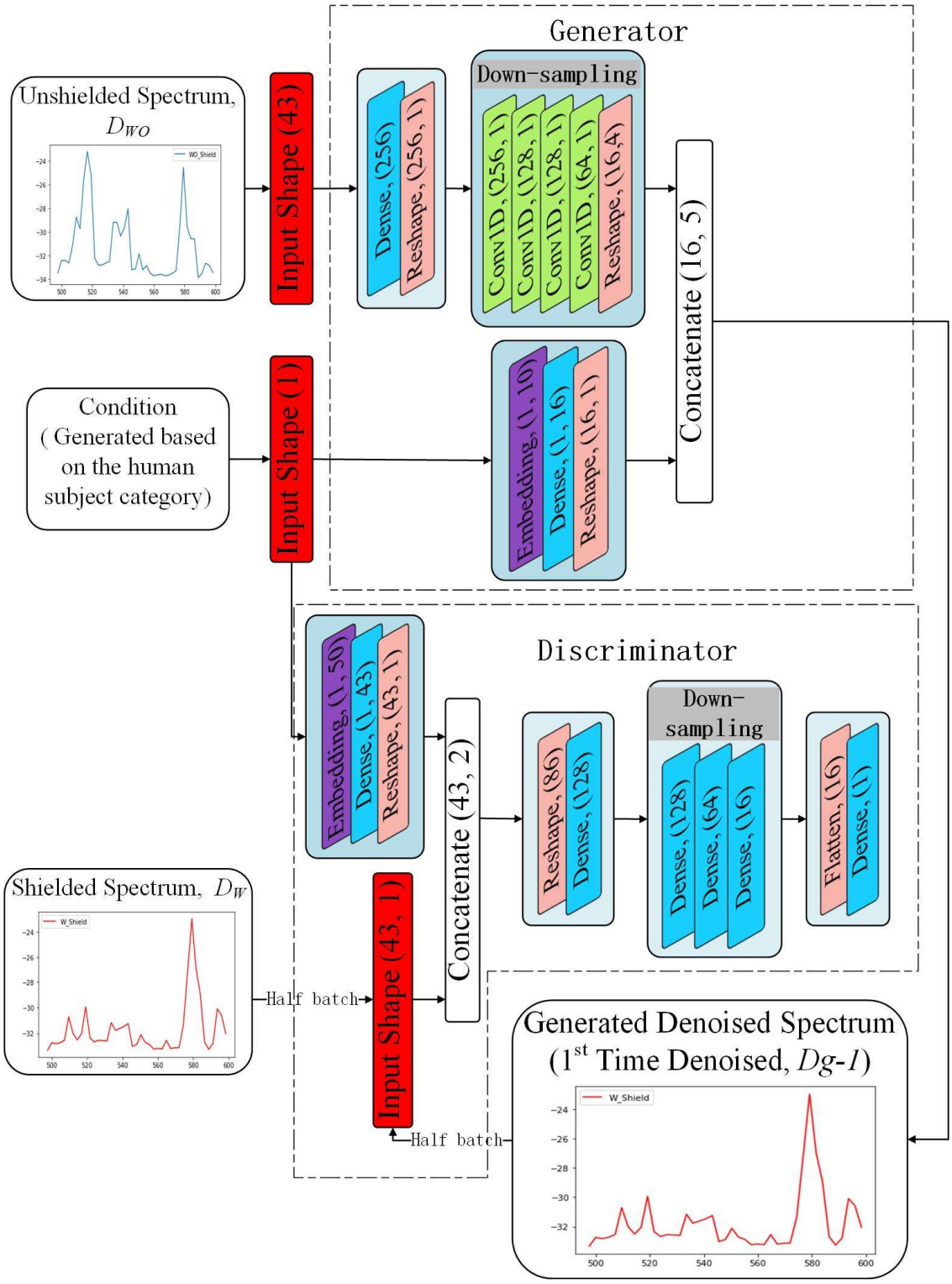

Figure 18. CGAN alternative framework 2: Removing the up-sampling process in the generator.

The synthesized spectra from the two alternatives and our proposed model are then compared with the target spectra in the with shield dataset D_W. The comparison result is evaluated by calculating the root mean square distance (RMSD), thus, the best framework setup should obtain the smallest RMSD value. In Table 5, it summarizes the training parameters and RMSD value calculated on the output spectra of the proposed model and the two alternatives.

Table 5. Training parameters and result summary

	Proposed model	**Alternative 1**	**Alternative 2**
Framework Highlight	With up-sampling & Dense layer	Convolutional layer in discriminator	Without up-sampling in generator
Epoch	140	200	220
Batch #	18	18	18
RMSD	0.0288	0.0338	0.0470

As shown in Table 5, the proposed model obtained the lowest RMSD value 0.0288, which indicates the setup has the best performance. Also, one thing worth noting from the table is that the proposed model requires the less amount of training epochs when comparing with the other two alternatives. With this being said, the correct CGAN framework setup can lead to efficient training process. In Figure 19, it shows the loss curve of training the alternative CGAN models with the parameter settings in Table 5.

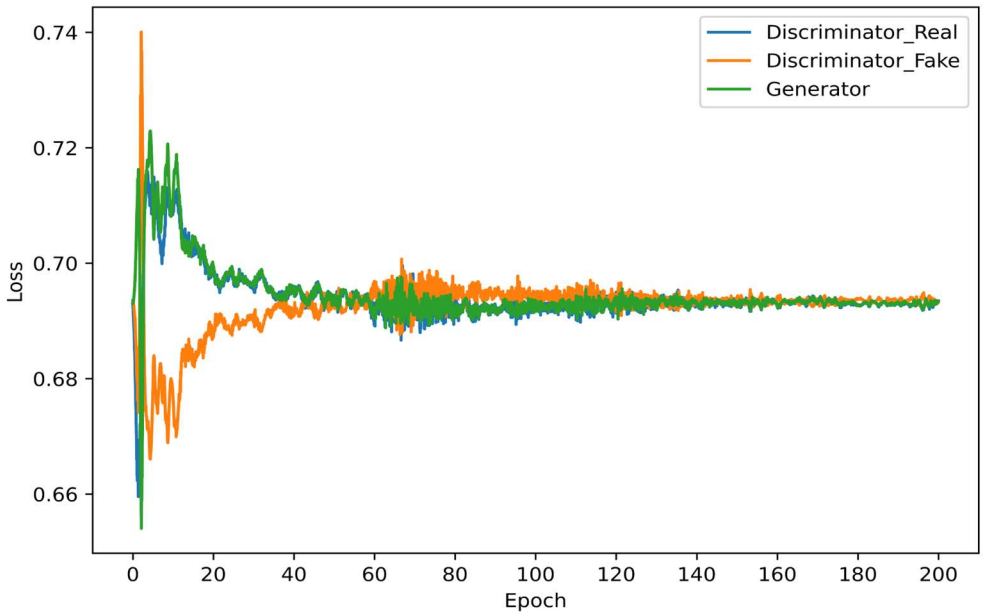

(a)

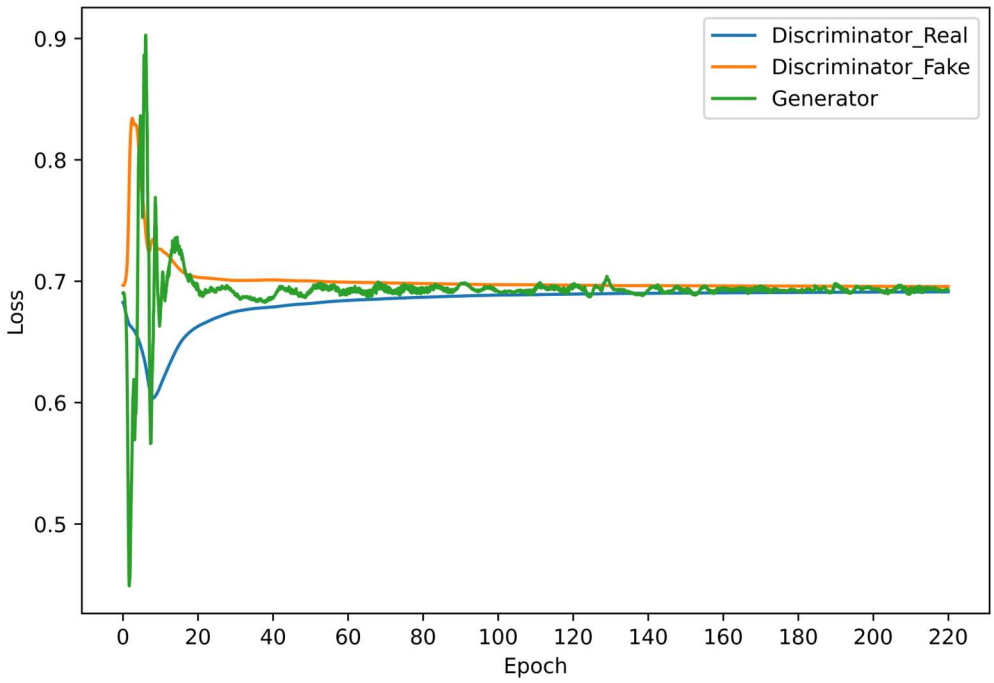

(b)

Figure 19. CGAN training loss curve, (a) CGAN model with fully convolutional layers in discriminator, (b) CGAN model without up-sampling process in generator.

In Figure 19, the blue and orange lines represent the loss value of discriminator while the green line represents the loss value of generator during training. The Figure 19 (a) shows the generator curve is oscillating even at the end of CGAN training where the loss curve already converges. The unstable generator loss curve during training indicates the generator framework is not designed properly. In the Figure 19 (b), it appears that the discriminator loss curve does not oscillate at the beginning of the training, which indicates the discriminator is not fully trained since the discriminator output on the generated and real spectrum are not challenging each other. The discriminator is only learning when the two loss curves are oscillating and against each other. The poor training result shown in Figure 19 (b) is caused by the nature of fully convolutional layer, since it tends to force the input share the parameters when learning the relationship of the input and output. With fewer parameters being used during the discriminator training, the spectrum data points quantity appears to be not enough, which results in the Dense layer to be a better option to fit our data type and shape.

4.4 Evaluation of Synthesized Spectrum

The SVM classifier is applied to evaluate the quality of the synthesized spectrum D_{g-1} and D_{g-2}, and the F1 scores are used as the main evaluation criteria. The SVM is trained on the training dataset in D_W to classify two human subjects. Figure 20 shows the trained SVM classifier performance on the testing dataset in D_W, which obtained a F1 score of 0.967.

However, with the two generated spectrum datasets D_{g-1} and D_{g-2}, the same trained SVM classifier shows higher score of 1.0 when identifying the two human

subjects on both datasets as shown in figure 21. This indicates that the synthesized spectrum outperformed the physical shielded spectrum in terms of subject classification accuracy.

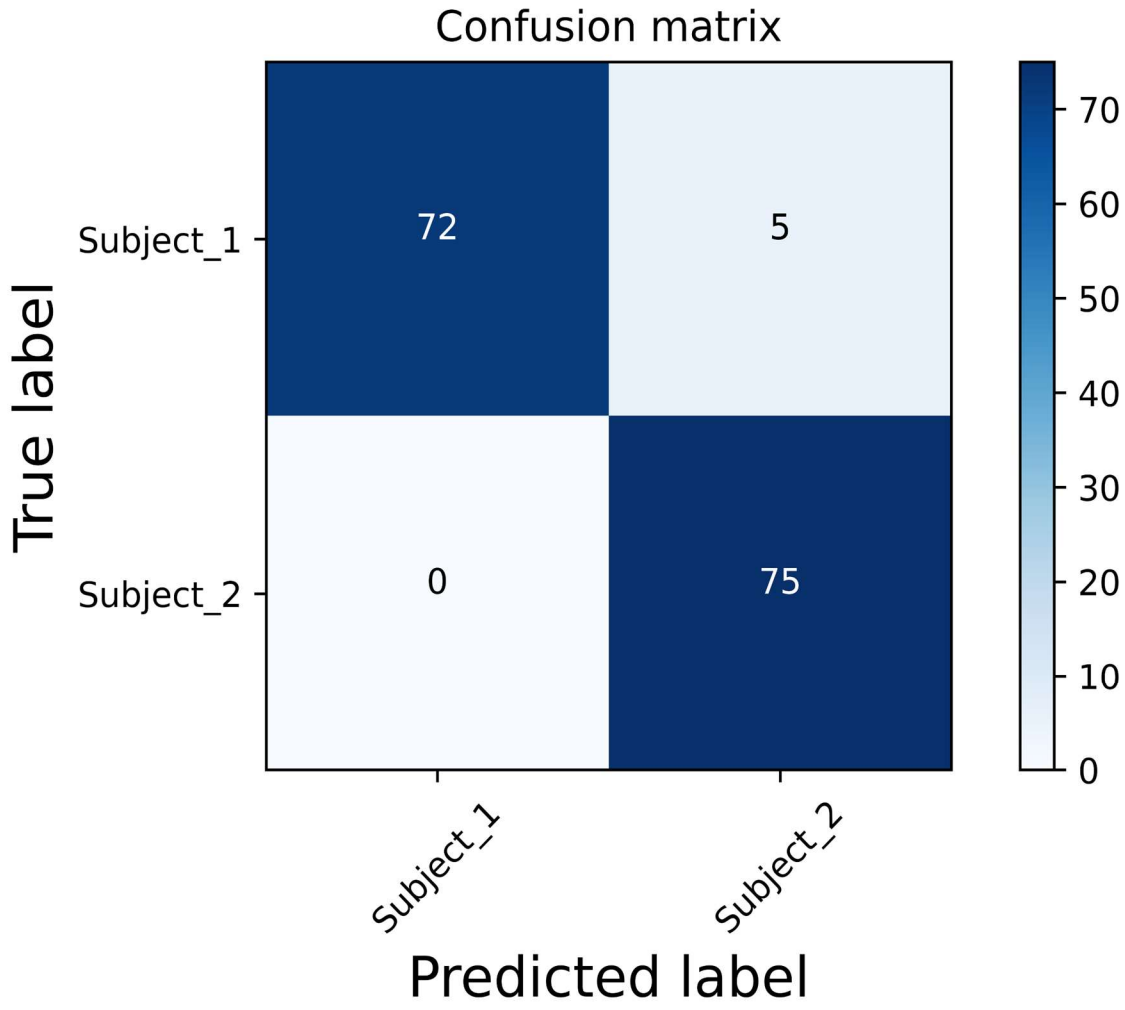

Figure 20. SVM classifier confusion matrix on $\boldsymbol{D_W}$ testing dataset.

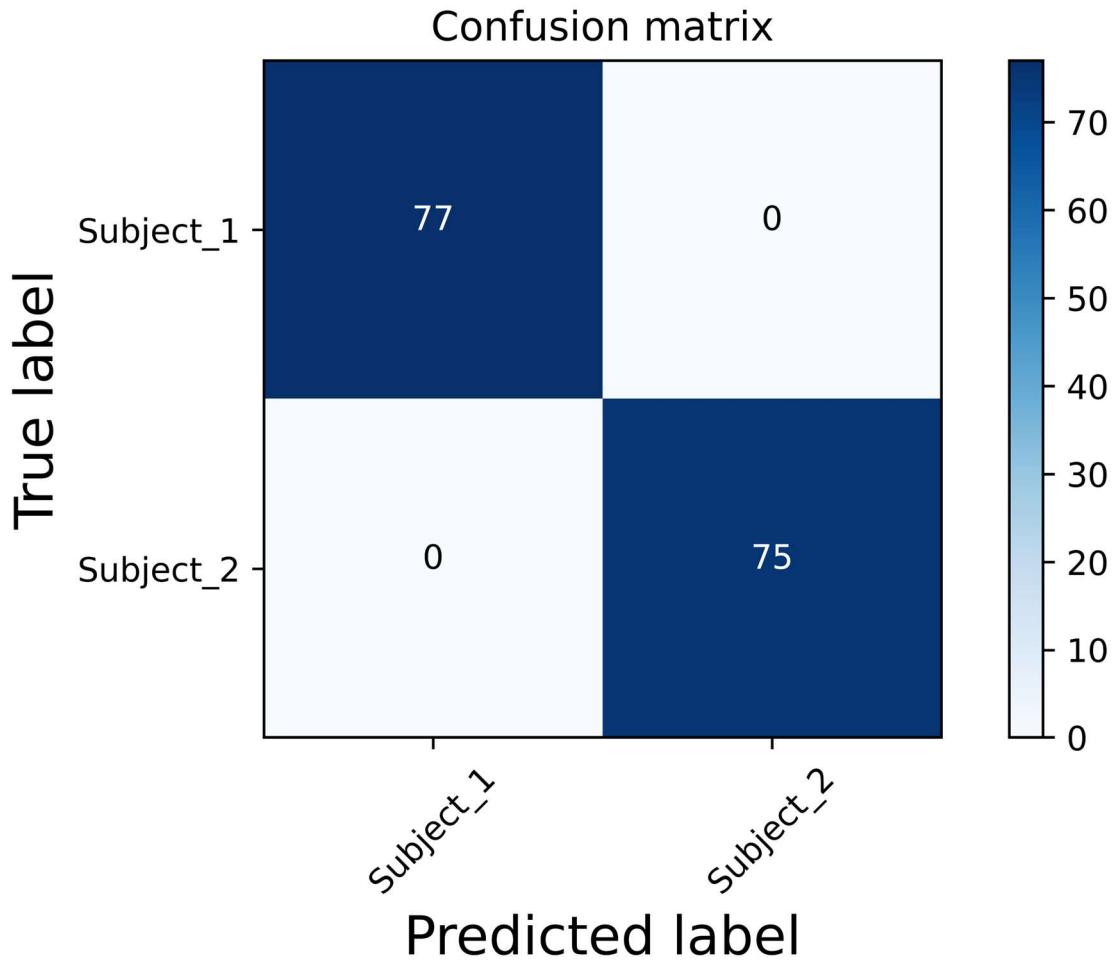

Figure 21. SVM classifier confusion matrix on $\boldsymbol{D_{g-1}}$ and $\boldsymbol{D_{g-2}}$ testing dataset

The SVM classifier is intended and trained to evaluate the generator performance based on the results of human subject identification. The initial expectation of the synthesized spectrum $D_{g-1}$and D_{g-2} is to maintain the same level of classifying accuracy as dataset D_W. However, the result shows that the two synthesized spectrum datasets obtained higher score from the classifier, which implies that the CGAN training is successful and the generator performance exceeds the expectation.

The SVM model classifies the spectra of human subject 1 & 2 based on the pattern of their human signatures, hence the classification accuracy is highly depending on the SNR of the human signature in the spectrum. The better quality and greater proportion of human signature exists in the spectrum would result in higher classification accuracy. In our research, the CGAN achieved the human signature extraction by simulating the physical shielding effect as expected. Furthermore, with the synthesized spectrum obtaining higher classification accuracy, it implies that the SNR in the synthesized spectrum is higher than in the target physical shielded spectrum. This may be caused by the additional denoising feature that is achieved during the generator training process due to the nature of the powerful machine learning technic and the way we setup the generator structure. In the real world, the data we captured are often heavily imbalanced, which always result in errors on classification. The up-sampling process in the generator structure has the ability of adjusting the data weights based on the features that are extracted from the down-sampling process, which could lead to the useful features weigh differently than in the target spectrum. The experiment result implies that this data points weight altering behavior has a positive impact to the spectrum, thus, we can come to a conclusion that our CGAN model grants the spectrum an improvement on the SNR. With the feature extraction and denoising feature, the synthesized spectrum in D_{g-1} and D_{g-2} both contain human signature with higher SNR than the shielded spectrum in D_W, which explains the higher scores gained on the SVM classification.

One thing should be noted is that the without up-sampling CGAN model denoised spectrum always obtained similar F1 score as the physically shielded spectrum obtained.

This further implies that the up-sampling process in the proposed model improves the denoising function by solving the data imbalance issue in the captured raw data.

CHAPTER FIVE
SUMMARY

5.1 Conclusion

In this thesis, a CGAN model is proposed to learn from physical shielding effect and create digital shielding effect to extract and denoise human signature on RF spectrum for human subject identification. In order to present the human signature in a compact and efficient way, the RF spectrum is analyzed by SHAP method to obtain the most human impacted frequency range. The CGAN can be applied multiple times to achieve different levels of denoising. The synthetic RF spectrums are evaluated by SVM classifier and proven to be accurately generated, effective to human identification, and containing adequate human signature information.

The experiment result shows that our CGAN model has the ability of generating the spectrum contains even higher SNR than the physically shielded spectrum. It indicates that with correct and efficient framework setup, the CGAN denoising method is able to outperform the mechanical denoising methods. Furthermore, our CGAN model successfully surpass many other GAN denoising techniques by obtaining even higher quality spectrum than the training target.

5.1 Future Work

This thesis is only focused on generating the synthetic denoised human spectrum, the classifier is used to evaluate the generated spectrum quality. The future research direction could be focusing on discovering the nature of human RF spectrum generation and radiation. To be more specific, with the RF spectrum denoising and human signature

extraction feature achieved, we can dig deeper into the field to study the cause of human spectrum signature variants and commons from different groups of human subjects, or the human generated electromagnetic field existence and impact factor. With this being said, unsupervised machine learning technique such as clustering may be adopted to this research in the future for classification purpose.

REFERENCES

[1] A.K. Jain, K. Nandakumar and A. Ross, " 50 years of biometric research: Accomplishments, challenges, and opportunities. " Pattern Recognit. Lett, 2016, 79, 80–105.

[2] C. Zeng and H. Ma, "Human detection using multi-camera and 3D scene knowledge," 2011 18th IEEE International Conference on Image Processing, 2011, pp. 1793-1796, doi: 10.1109/ICIP.2011.6115810.

[3] T. Taipalus and J. Ahtiainen, "Human detection and tracking with knee-high mobile 2D LIDAR," 2011 IEEE International Conference on Robotics and Biomimetics, 2011, pp. 1672-1677, doi: 10.1109/ROBIO.2011.6181529.

[4] V. C. Chen, "Detection and analysis of human motion by radar," 2008 IEEE Radar Conference, 2008, pp. 1-4, doi: 10.1109/RADAR.2008.4721059.

[5] S. Chang, N. Mitsumoto and J. W. Burdick, "An algorithm for UWB radar-based human detection," 2009 IEEE Radar Conference, 2009, pp. 1-6, doi: 10.1109/RADAR.2009.4976999.

[6] K. Hashimoto, N. Yoshiike, and K. Morinaka, "Human occupancy detection method and system for implementing the same," U.S. Patent No. 5,703,367. 30, Dec. 1997.

[7] T. Zhang, T. Song, D. Chen, T. Zhang and J. Zhuang, "WiGrus: A Wifi-Based Gesture Recognition System Using Software-Defined Radio," in IEEE Access, vol. 7, pp. 131102-131113, 2019, doi: 10.1109/ACCESS.2019.2940386.

[8] R. Zhang, X. Jing, “Device-Free Human Identification Using Behavior Signatures in WiFi Sensing.” Sensors, 21.17 (2021): 5921–. Web.

[9] J. Liu, H. Mu, A. Vakil, R. Ewing, X. Shen, E. Blasch, J. Li, "Human Occupancy Detection via Passive Cognitive Radio," Sensors, vol. 20, no. 15, 4248, Jul. 2020.

[10] Zweifel, Nadina O., and Mitra J. Z. Hartmann. “Defining ‘active Sensing’ through an Analysis of Sensing Energetics: Homeoactive and Alloactive Sensing.” Journal of Neurophysiology, vol. 124, no. 1, 2020, pp. 40–48, https://doi.org/10.1152/jn.00608.2019.

[11] Ortiz, Abigail, et al. “Identifying Patient-Specific Behaviors to Understand Illness Trajectories and Predict Relapses in Bipolar Disorder Using Passive Sensing and Deep Anomaly Detection: Protocol for a Contactless Cohort Study.” BMC Psychiatry,

vol. 22, no. 1, BioMed Central Ltd, 2022, pp. 288–288, https://doi.org/10.1186/s12888-022-03923-1.

[12] Wade, Natasha E., et al. “Passive Sensing of Preteens’ Smartphone Use: An Adolescent Brain Cognitive Development (ABCD) Cohort Substudy.” JMIR Mental Health, vol. 8, no. 10, JMIR Publications, 2021, pp. e29426–e29426, https://doi.org/10.2196/29426.

[13] Wade, Natasha E., et al. “Passive Sensing of Preteens’ Smartphone Use: An Adolescent Brain Cognitive Development (ABCD) Cohort Substudy.” JMIR Mental Health, vol. 8, no. 10, JMIR Publications, 2021, pp. e29426–e29426, https://doi.org/10.2196/29426.

[14] Iannizzotto, Giancarlo, et al. “A Perspective on Passive Human Sensing with Bluetooth.” Sensors (Basel, Switzerland), vol. 22, no. 9, MDPI AG, 2022, p. 3523–, https://doi.org/10.3390/s22093523.

[15] Zou, H., Zhou, Y., Yang, J., et al., “Freedetector: device-free occupancy detection with commodity WiFi”, 2017 IEEE Int. Conf. on Sensing, Communication and Networking (SECON Workshops), San Diego, CA,2017, pp. 1–5

[16] Liu, Jiao, et al. “Human Activity Sensing with Wireless Signals: A Survey.” Sensors (Basel, Switzerland), vol. 20, no. 4, MDPI, 2020, p. 1210–, https://doi.org/10.3390/s20041210.

[17] Lisowski, Mateusz, et al. “Structural Damage Detection Using Wireless Passive Sensing Platform Based on RFID Technology: Structural Damage Detection Using Wireless Passive Sensing Platform.” Structural Control and Health Monitoring, vol. 23, no. 8, 2016, pp. 1135–46, https://doi.org/10.1002/stc.1826.

[18] Li, Wenda, et al. “WiFi-Based Passive Sensing System for Human Presence and Activity Event Classification.” IET Wireless Sensor Systems, vol. 8, no. 6, The Institution of Engineering and Technology, 2018, pp. 276–83, https://doi.org/10.1049/iet-wss.2018.5113.

[19] Mohtadifar, Masoud, et al. “Acoustic- and Radio-Frequency-Based Human Activity Recognition.” Sensors (Basel, Switzerland), vol. 22, no. 9, MDPI AG, 2022, p. 3125–, https://doi.org/10.3390/s22093125.

[20] Buades, A.; Coll, B.; Morel, J-M. A non-local algorithm for image denoising. Computer Vision and Pattern Recognition. IEEE Computer Society Conference on; IEEE; 2005. p. 60-65

[21] Coupé, Pierrick, et al. “Fast Non Local Means Denoising for 3D MR Images.” Medical Image Computing and Computer-Assisted Intervention – MICCAI 2006, Springer Berlin Heidelberg, pp. 33–40, https://doi.org/10.1007/11866763_5.

[22] Rajan J, Veraart J, Van Audekerke J, Verhoye M, Sijbers J. Nonlocal maximum likelihood estimation method for denoising multiplecoil magnetic resonance images. Magnetic Resonance imaging. 2012; 30(10):1512–1518. [PubMed: 22819583]

[23] Tian, Lin, et al. “A Novel Denoising Algorithm for Medical Images Based on the Non-convex Non-local Similar Adaptive Regularization.” IET Image Processing, vol. 15, no. 8, Wiley, 2021, pp. 1702–11, https://doi.org/10.1049/ipr2.12138.

[24] Veraart, Jelle, et al. “Denoising of Diffusion MRI Using Random Matrix Theory.” NeuroImage (Orlando, Fla.), vol. 142, Elsevier Inc, 2016, pp. 394–406, https://doi.org/10.1016/j.neuroimage.2016.08.016.

[25] Breitling, Johannes, et al. “Adaptive Denoising for Chemical Exchange Saturation Transfer MR Imaging.” NMR in Biomedicine, vol. 32, no. 11, Wiley Subscription Services, Inc, 2019, p. e4133–n/a, https://doi.org/10.1002/nbm.4133.

[26] Tan J., Ung M., Cheng C., Greene C.S. “Unsupervised feature construction and knowledge extraction from genome-wide assays of breast cancer with denoising autoencoders.” Pac Symp Biocomput. 2015:132–143.

[27] Tan J, Hammond JH, Hogan DA, Greene CS. “ADAGE-based integration of publicly available Pseudomonas aeruginosa gene expression data with denoising autoencoders illuminates microbe-host interactions.” mSystems. 2016;1:e00025–15.

[28] Wang, Jun, et al. “Denoising Autoencoder, A Deep Learning Algorithm, Aids the Identification of A Novel Molecular Signature of Lung Adenocarcinoma.” Genomics, Proteomics & Bioinformatics, vol. 18, no. 4, Elsevier B.V, 2020, pp. 468–80, https://doi.org/10.1016/j.gpb.2019.02.003.

[29] Ram, Shobha Sundar, et al. “Sparsity-based Autoencoders for Denoising Cluttered Radar Signatures.” IET Radar, Sonar & Navigation, vol. 15, no. 8, Wiley, 2021, pp. 915–31, https://doi.org/10.1049/rsn2.12065.

[30] Goodfellow I, Pouget-Abadie J, Mirza M, Xu B, Warde-Farley D, Ozair S, Courville A, Bengio Y, “Generative adversarial nets.” Advances in neural information processing systems, 2014, pp 2672– 2680.

[31] Odena A, “Semi-supervised learning with generative adversarial networks.” 2016 arXiv:160601583

[32] Odena A, Olah C, Shlens J “Conditional image synthesis with auxiliary classifier gans.” 2016, arXiv:161009585

[33] Reed S, Akata Z, Yan X, Logeswaran L, Schiele B, Lee H, “Generative adversarial text to image synthesis.” In: Proceedings of the 33rd International Conference on Machine Learning, 2016, vol 3.

[34] Reed SE, Akata Z, Mohan S, Tenka S, Schiele B, Lee H, “Learning what and where to draw.” Advances in Neural Information Processing Systems, 2016, pp 217–225.

[35] Isola P, Zhu JY, Zhou T, Efros AA, “Image-to-image translation with conditional adversarial networks.” 2016, arXiv:161107004.

[36] Yi, Xin, and Paul Babyn. “Sharpness-Aware Low-Dose CT Denoising Using Conditional Generative Adversarial Network.” Journal of Digital Imaging, vol. 31, no. 5, Springer International Publishing, 2018, pp. 655–69, https://doi.org/10.1007/s10278-018-0056-0.

[37] Chen, Zailiang, et al. “DN-GAN: Denoising Generative Adversarial Networks for Speckle Noise Reduction in Optical Coherence Tomography Images.” Biomedical Signal Processing and Control, vol. 55, Elsevier Ltd, 2020, p. 101632–, https://doi.org/10.1016/j.bspc.2019.101632.

[38] Yang, Qingsong, et al. “Low-Dose CT Image Denoising Using a Generative Adversarial Network with Wasserstein Distance and Perceptual Loss.” IEEE Transactions on Medical Imaging, vol. 37, no. 6, IEEE, 2018, pp. 1348–57, https://doi.org/10.1109/TMI.2018.2827462.

[39] Li, Ziyu, et al. “High-fidelity Fast Volumetric Brain MRI Using Synergistic Wave-controlled Aliasing in Parallel Imaging and a Hybrid Denoising Generative Adversarial Network (HDnGAN).” Medical Physics (Lancaster), vol. 49, no. 2, 2022, pp. 1000–14, https://doi.org/10.1002/mp.15427.

[40] Al-Mualem, Ziareena A., and Carlos R. Baiz. “Generative Adversarial Neural Networks for Denoising Coherent Multidimensional Spectra.” The Journal of Physical Chemistry. A, Molecules, Spectroscopy, Kinetics, Environment, & General Theory, vol. 126, no. 23, American Chemical Society, 2022, pp. 3816–25, https://doi.org/10.1021/acs.jpca.2c02605.

[41] Radford, A., Metz, L., Chintala, S. “Unsupervised Representation Learning with Deep Convolutional Generative Adversarial Networks.” arXiv, 2016, arXiv:1511.06434v2.

[42] D. Janzing, L. Minorics, P. Bloebaum, “Feature relevance quantification in explainable AI: A causal problem”, Proceedings of the Twenty Third International Conference on Artificial Intelligence and Statistics, PMLR 108:2907-2916, 2020.

[43] I. J. Goodfellow et al., “Generative Adversarial Networks,” 2014.

[44] Mirza M, Osindero S, “Conditional generative adversarial nets,” 2014. arXiv:14111784 [cs.LG].

[45] D. M. Abdullah, A. M. Abdulazeez, “Machine learning applications based on SVM classification a review,” Qubahan Academic Journal, 2021, 1(2), pp. 81-90.

[46] Ran, Maosong, et al. “Denoising of 3D Magnetic Resonance Images Using a Residual Encoder–decoder Wasserstein Generative Adversarial Network.” Medical Image Analysis, vol. 55, Elsevier B.V, 2019, pp. 165–80, https://doi.org/10.1016/j.media.2019.05.001.